The cooling capabilities of C_2F_6/C_3F_8 saturated fluorocarbon blends for the ATLAS silicon tracker

2015 JINST 10 P03027

(http://iopscience.iop.org/1748-0221/10/03/P03027)

PUBLISHED BY IOP PUBLISHING FOR SISSA MEDIALAB

RECEIVED: *November 26, 2014*
REVISED: *January 29, 2015*
ACCEPTED: *February 6, 2015*
PUBLISHED: *March 26, 2015*

The cooling capabilities of C_2F_6/C_3F_8 saturated fluorocarbon blends for the ATLAS silicon tracker

R. Bates,[a] **M. Battistin,**[b] **S. Berry,**[b] **A. Bitadze,**[a] **P. Bonneau,**[b] **N. Bousson,**[c] **G. Boyd,**[d] **J. Botelho-Direito,**[b] **O. Crespo-Lopez,**[b] **B. DiGirolamo,**[b] **M. Doubek,**[e] **D. Giugni,**[b] **G. Hallewell,**[c,1] **D. Lombard,**[b] **S. Katunin,**[f] **S. McMahon,**[g] **K. Nagai,**[h] **D. Robinson,**[i] **C. Rossi,**[j] **A. Rozanov,**[c] **V. Vacek**[e] **and L. Zwalinski**[b]

[a] *SUPA School of Physics and Astronomy, University of Glasgow, Kelvin Building, University Avenue, Glasgow, G12 8QQ, U.K.*
[b] *CERN, 1211 Geneva 23, Switzerland*
[c] *Centre de Physique des Particules de Marseille, Aix-Marseille Université, CNRS/IN2P3, 163 Avenue de Luminy, 13288 Marseille Cedex 09, France*
[d] *The Homer L. Dodge Department of Physics and Astronomy, University of Oklahoma, 440 West Brooks Street, Norman, OK 73019, U.S.A.*
[e] *Czech Technical University in Prague, Department of Applied Physics, Technická 4, 166 07 Prague 6, Czech Republic*
[f] *B.P. Konstantinov Petersburg Nuclear Physics Institute (PNPI), Gatchina, Leningrad district, 188300 St. Petersburg, Russia*
[g] *Rutherford Appleton Laboratory — Science & Technology Facilities Council, Harwell Science and Innovation Campus, Didcot OX11 OQX, U.K.*
[h] *Department of Physics, Oxford University, Keble Road, Oxford OX1 3RH, U.K.*
[i] *Department of Physics and Astronomy, Cavendish Laboratory, University of Cambridge, J.J. Thompson Avenue, Cambridge, CB3 0HE, U.K.*
[j] *Institue of Physics of the Academy of Sciences of the Czech Republic, Na Slovance 2, 182 21 Prague 8, Czech Republic*

E-mail: gregh@cppm.in2p3.fr

[1] Corresponding author.

doi:10.1088/1748-0221/10/03/P03027

2015 JINST 10 P03027

ABSTRACT: We investigate and address the performance limitations of the ATLAS silicon tracker fluorocarbon evaporative cooling system operation in the cooling circuits of the barrel silicon microstrip (SCT) sub-detector. In these circuits the minimum achievable evaporation temperatures with C_3F_8 were higher than the original specification, and were thought to allow an insufficient safety margin against thermal runaway in detector modules subject to a radiation dose initially foreseen for 10 years operation at LHC.

We have investigated the cooling capabilities of blends of C_3F_8 with molar admixtures of up to 25% C_2F_6, since the addition of the more volatile C_2F_6 component was expected to allow a lower evaporation temperature for the same evaporation pressure.

A custom built recirculator allowed the *in-situ* preparation of C_2F_6/C_3F_8 blends. These were circulated through a representative mechanical and thermal setup reproducing an as-installed ATLAS SCT barrel tracker cooling circuit. Blend molar compositions were verified to a precision of 3.10^{-3} in a custom ultrasonic instrument.

Thermal measurements in a range of C_2F_6/C_3F_8 blends were compared with measurements in pure C_3F_8. These indicated that a blend with 25% C_2F_6 would allow a reduction in evaporation temperature of around 9°C to below -15°C, even at the highest module power dissipations envisioned after 10 years operation at LHC. Such a reduction would allow more than a factor two in safety margin against temperature dependant leakage power induced thermal runaway.

Furthermore, a blend containing up to 25% C_2F_6 could be circulated without changes to the on-detector elements of the existing ATLAS inner detector evaporative cooling system.

KEYWORDS: Detector cooling and thermo-stabilization; Gas systems and purification; Materials for gaseous detectors

2015 JINST 10 P03027

Contents

1 Introduction

1.1 Motivation

During initial operation of the ATLAS silicon tracker fluorocarbon evaporative cooling system a limitation in performance of the cooling circuits of the barrel silicon microstrip (SCT) subdetector was encountered. The minimum achievable evaporation temperatures with C_3F_8 [*octafluoropropane*: R218; molecular weight (mw) = 188] were higher than the original specification due to greater than expected pressure drops in inaccessible regions of the exhaust vapour return tubing, and were thought to allow an insufficient safety margin against thermal runaway once the detector modules had been subjected to a radiation dose approaching that initially foreseen in their expected 10 year operational lifetime at LHC.

Prior estimates of the evolution of depletion voltage and leakage current suggested that an evaporation temperature of -15°C would be required for an adequate safety margin against thermal runaway under the expected operating profile. Since laboratory measurements in a representative cooling circuit demonstrated that this temperature could not be achieved with pure C_3F_8 with return line parameters as in the installed ATLAS evaporative cooling system, we have investigated the cooling capabilities of blends of C_3F_8 with molar admixtures of up to 25% C_2F_6 [*hexafluoroethane*: R116; molecular weight (mw) = 138]. The addition of the lighter and more volatile C_2F_6

2015 JINST 10 P03027

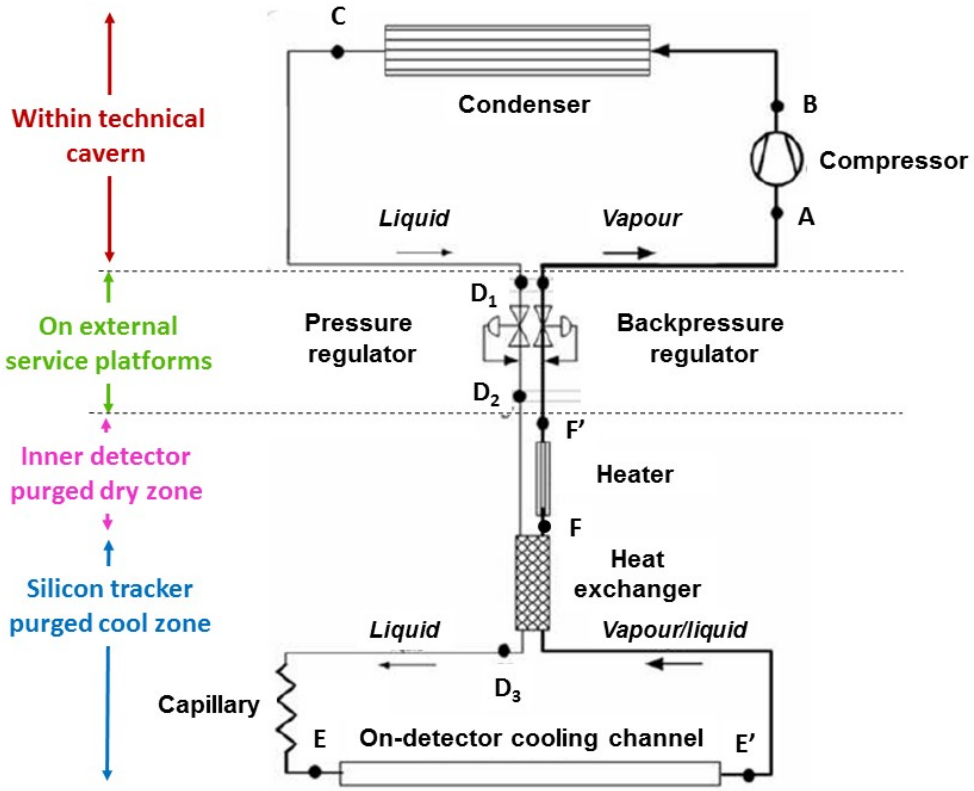

Figure 1. Principal components of the ATLAS ID evaporative cooling system schematically illustrated in the case of one of 204 parallel cooling circuits. In some circuits liquid is supplied through multiple capillaries to structures sharing a common exhaust.

component was expected to allow a lower evaporation temperature for the same evaporation pressure. Thermodynamic calculations suggested that a blend containing up to 25% C_2F_6 could be circulated without changes to the on-detector elements or the inaccessible liquid delivery and vapour exhaust systems of the existing ATLAS inner detector evaporative cooling system.

1.2 The ATLAS inner detector C_3F_8 evaporative cooling system

The ATLAS Inner Detector (ID) contains a multi-layer silicon tracker. In this tracker two independent subsystems are presently cooled by the evaporation of C_3F_8. Of these the Pixel detector is located close to the interaction point and comprises 3 cylindrical layers of silicon pixels with three disk-shaped layers at each end. The Semi-Conductor Tracker (SCT) surrounds the Pixel detector with 4 cylindrical barrel layers of silicon microstrip detectors, with a further nine disk-shaped layers at each end. These subsystems can collectively dissipate up to 60kW of heat after long term radiation damage as a result of operation at the CERN Large Hadron Collider (LHC). The evaporative cooling system circulates coolant through the Pixel and SCT detectors via 204 cooling circuits [1]. Figure 1 illustrates the principal components of the ATLAS C_3F_8 evaporative cooling system.

2015 JINST 10 P03027

Shared principal components of the system include compressors and a condenser. Individual circuit elements include liquid flow-defining pressure regulators (PRs), the on-detector capillaries and cooling tubes (or evaporators), followed — in order of fluid flow — by heat exchangers, electric heaters and evaporation pressure-defining back pressure regulators (BPRs).

In each cooling circuit, liquid refrigerant arrives through a 30 m uninsulated supply tube and is sub-cooled (segment $\mathbf{D_2D_3}$ in figure 1) in a heat exchanger by counter-flowing cold liquid/vapour exhausting from the on-detector cooling channel. The liquid PR is set to a fixed pressure to provide a mass flow of around 120% of that necessary for the maximum expected detector dissipation. Any liquid remaining at the output of the heat exchanger (point **F** in figure 1) must be evaporated in an electric heater (**FF'**) and the exhaust vapour temperature raised above the expected cavern dew point of 12°C to prevent condensation on the exterior un-insulated vapour exhaust tubing. The heaters are mounted close to the silicon tracker cold volume in the closed ID zone, which is flushed with dry CO_2 gas to prevent condensation. The evaporation pressure in the on-detector cooling tubes (and thereby the detector operating temperature) is set with a BPR located on a service platform around 30 m downstream of the heater.

The pressure drop in the exhaust system between the end of the on-detector cooling tube (**E'**) and the input of the BPR (**F'**) must be well understood and managed, or can result in an unacceptable increase in detector operating temperature, particularly at high power loads following operation at high accumulated radiation dose. The original design, in which the internal diameters of the exhaust tube, electric heaters and heat exchanges were chosen, assumed a maximum pressure drop over segment **E'FF'** of 470 mbar [1]. Operation with this exhaust pressure drop using C_3F_8 would result in a thermodynamic cycle similar to that shown in the pressure-enthalpy diagram of figure 2.

The thermodynamic cycle is composed of several state transitions occurring between successive indices, as detailed table 1.

The operating temperatures of the SCT and Pixel silicon substrates affect long term annealing processes which determine the increase in depletion voltage and leakage current (I_{leak}) under irradiation.

These silicon substrates will remain thermally stable only if the coolant temperature and thermal resistance are low enough to allow the heat generated by the front end electronics and substrate leakage current to be removed. Failure to maintain a sufficiently low temperature can result in 'thermal runaway' [2], a self-destructive *positive feedback* phenomenon where the self-heating product of substrate leakage current and applied depletion voltage can further increase I_{leak}.

It was believed that these concerns would be addressed by maintaining the temperature of the silicon substrates of the SCT and Pixel detectors below -7°C [3, 4] and 0°C [5] respectively. Expected thermal impedances through the support structures attaching the silicon modules to the coolant channels predicated a typical evaporation temperature of $\sim$ -25°C in the on-detector cooling channels for full power operation after the accumulation of radiation damage from 10 years of LHC operation under the original luminosity LHC assumptions [3–5]. This evaporation temperature was

[1] Model QTOGX 160/80 LM: Haug Kompressoren AG, Industriestrasse 6, CH-9015 St. Gallen, Switzerland maximum output (minimum aspiration) pressures of 17 (0.8) bar_{abs}; flow rate 120 m^3hr^{-1} C_3F_8 at P_{in} = 1.0 bar_{abs}, P_{out} = 17 bar_{abs}. A bank of seven parallel compressors is used, with typically 5 in simultaneous service.

[2] This temperature is chosen to ensure a safety margin above the ATLAS cavern dew point of 12°C.

[3] Model 26-2310-28-205, Emerson-Tescom, 12616 Industrial Boulevard, Elk River, MN 55330 U.S.A.

2015 JINST 10 P03027

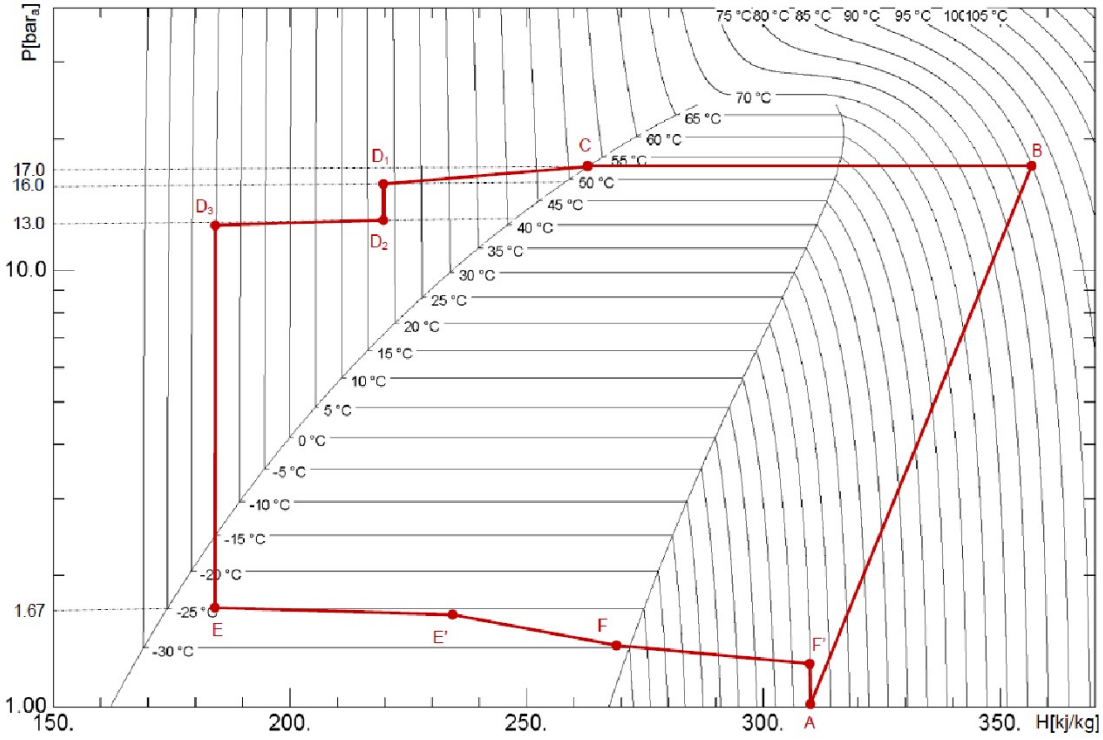

Figure 2. Target pressure-enthalpy diagram for the ATLAS ID evaporative cooling system operation with C_3F_8 (table 1).

the original design specification for the ATLAS silicon tracker cooling system [1], corresponding to an evaporation pressure of 1.67bar$_{abs}$ with C_3F_8, as illustrated in the pressure-enthalpy diagram of figure 2. More recent — and reduced — estimates of the 10 year integrated luminosity at LHC have suggested that a higher SCT silicon module substrate temperature of 10°C could assure a safety factor of two against leakage power induced thermal runaway (as reported in [6]). These module operating temperatures would be maintained by a corresponding evaporation temperature of -15°C in the SCT on-detector cooling channels.

1.3 Measured limitations of C_3F_8 evaporative cooling for the SCT barrel bi-stave circuits

Previous studies made in a test structure representing an SCT cooling channel — (referred to hereafter as a "bi-stave") had shown [6] evaporation at the design pressure of 1.67 bar$_{abs}$ to be unachievable over a wide range of power dissipation in the currently-configured C_3F_8 evaporative cooling system, due to higher than expected pressure drops in inaccessible regions of the exhaust vapour return system (segment **E'FF'** in figure 2).

Figures 3 and 4 illustrate the test structure that was used to emulate a barrel SCT cooling circuit and which has been retained and extended for the present study. Spare parts for barrel SCT cooling circuits were used to build the bi-stave test structure, including the on-detector cooling tubes, the

2015 JINST 10 P03027

Table 1. Transition points on the enthalpy-pressure diagram of figure 1.

Transition	Physical State and location
A→B	Pressure and temperature rise from (1 bar_{abs}, 20°C) at the input of the oil-less two-stage compressor,[1] to (17 bar_{abs}, 90°C) at its output.
B→C	Subsequent cooling and condensation of the C_3F_8vapour;
C→D_1	Sub-cooling of the condensed C_3F_8 liquid in a storage tank in the ATLAS technical cavern and along its 150m delivery path to flow division racks located on service platforms mounted on the detector.
D_1 →D_2	Pressure drop over the PRs on the liquid distribution manifolds and delivery tubes to the inner detector cold volume.
D_2 → D_3	Sub-cooling of the arriving C_3F_8 liquid through counterflow heat exchange with exhausting liquid/vapour (segment **EF**), allowing the use of a greater fraction of the available enthalpy of evaporation to cool the detector.
D_3 → E	Pressure drop across the capillary from 13 bar_{abs} to the evaporation pressure of 1.67 bar_{abs}.
E→E'	Removal of heat from the detector via evaporation of liquid C_3F_8 in the on-detector cooling channel.
E'→F	Enthalpy consumed in the heat exchanger to sub-cool the arriving liquid (segment $\mathbf{D_2D_3}$).
F→F'	Evaporation of any liquid remaining at the output of the heat exchanger, and the raising of the vapour temperature to 20°C[2] using an electric heater.
F'→A	Combined pressure drop across the BPR[3] defining the on-detector evaporation temperature and the tubing returning the vapour from the ATLAS service platforms to the compressor input.

module attachment blocks [7], the heater, subcooling heat exchanger and capillaries, to which additional instrumentation was added for measurement of the temperature and pressure profiles.

The "on-detector" part of the test structure consists of two U-shaped "staves" sharing a common exhaust manifold, together with the local liquid delivery and exhaust tubing. In the installed detector such "on-detector" components lie within the pseudorapidity acceptance of the silicon tracker; their associated radiation length (%X0) must be reduced as far as possible, consistent with operating practicality, to minimise background and multiple scattering. Other elements, including liquid subcooling heat exchangers, exhaust heaters and the larger diameter liquid delivery and exhaust vapour tubing are positioned outside of this critical zone at larger radius.

2015 JINST 10 P03027

In each stave two straight cupro-nickel tubes of 4.06 mm internal diameter and 70 μm wall thickness are attached in series with a 180° turn at the midpoint. Liquid coolant flow is equally divided between the two staves through the use of a pair of capillaries of nominal internal diameter 0.76 mm and length 72 cm.

The cooling tube of each stave has a combined length of 300 cm and cools 24 dummy modules: ceramic substrates of length 6.2 cm and width 2.5 cm with deposited zig-zag metallic heating elements of resistance 161 $\pm$ 0.2 Ω. Heat from the dummy modules is directed through a film of GC-ELECTRONICS® 10-8108[4] thermal grease to standard SCT aluminium alloy coupling blocks [7] which are silver soldered to the cooling tubes.

Temperature sensors are attached at various positions in the liquid supply and vapour exhaust tubing, as indicated in figure 3 and to the Cu-Ni tubes of the staves at positions midway between modules. The overall uncertainty in temperature measurements was estimated to be $\pm$ 0.35°C, based on the intrinsic sensor resolution,[5] ADC calibration and the standard deviation in measured temperature values under zero power operation with a flow of around 12.7 g.s^{-1} C_3F_8 and a back-pressure of 1.2 bar$_{abs}$.[6] The latter uncertainty includes the effects of small variations in temperature sensor attachment to the cooling tube.

The pressures in the system were measured with electronic transducers.[7] The pressure upstream of the capillaries was measured to a precision of $\pm$ 15 mbar[7] by transducers with 30 bar full scale. Pressures downstream of the capillaries, at the half-way points on each stave, on the common exhaust and at the input of the BPR were measured to a precision of $\pm$ 5 mbar[7] by transducers with 10 bar full scale. In all tests both staves were run in parallel under identical flow and power conditions: the overall exhaust system pressure drop is thus determined by the combined exhaust flow, in the same way as in the installed SCT barrel bi-staves.

The SCT bi-stave test structure was housed in a plexiglass box externally insulated with 5 cm of Armaflex® insulation and flushed with dry air. As in the SCT detector, the liquid refrigerant delivered to each capillary was locally sub-cooled to a temperature of around -15°C in a heat exchanger cooled by counter-flowing cold exhaust liquid/vapour. A combined fixed liquid flow of 12.7 $\pm$ 0.3 g s^{-1} [8] was established with the upstream liquid PR set to 13bar$_{abs}$ and injected into the two capillaries, irrespective of the heat dissipation in the structure. The PR was followed by a heat exchanger operating with water at 17°C to stabilise the liquid temperature at the input of the

[4]Thermal conductivity 0.75 Wm^{-1}K^{-1}, similar to that of Dow Corning 340 used in the SCT detector (0.67 Wm^{-1}K^{-1}).

[5]104JT025 NTC ("negative temperature coefficient) kapton embedded (max. total thickness 500 μm) thermistors: 100 kΩ at 25 °C: Semitec Corp. 7-7 Kinshi 1-Chome, Sumida-ku, Tokyo 130-8512, Japan. Intrinsic precision $\pm$ 1% (1kΩ) at 25°C. Resistance variation with absolute temperature T of the form $R_1 = R_2.e^{B.\left(\frac{1}{T_1}-\frac{1}{T_2}\right)}$ where B= 4390 $\pm$ 1%. These two effects yield a combined intrinsic temperature error of $\pm$ 0.21°C.

[6]The difference in pressure measured between the inlet and exit of a stave ([$P_{A(B)1}$]-[$P_{A(B)3}$] in figure 3) was around 100 mbar, implying a difference in saturation temperature of 1.5°C. However in the zero power condition the thermal conductivity of the Cu-Ni tube was able to equilibrate the temperature to within $\pm$ 0.28°C (standard deviation of around 100 measurements on each of 25 tube wall temperature sensors taken under stable flow conditions), masking the effect of the dynamic pressure drop seen at higher applied power levels.

[7]Model PAA33X pressure transducer. Keller AG: St. Gallerstrasse 119 CH-8404 Winterthur Switzerland. Precision $\pm$ 0.05% of full scale.

[8]Based on the standard deviation of around 400 flow measurements over a period of around 2 hours, during which thermal data were taken at 4 power ratings (0W, 6W, 9W and 10.5W per emulated module) at the same backpressure.

2015 JINST 10 P03027

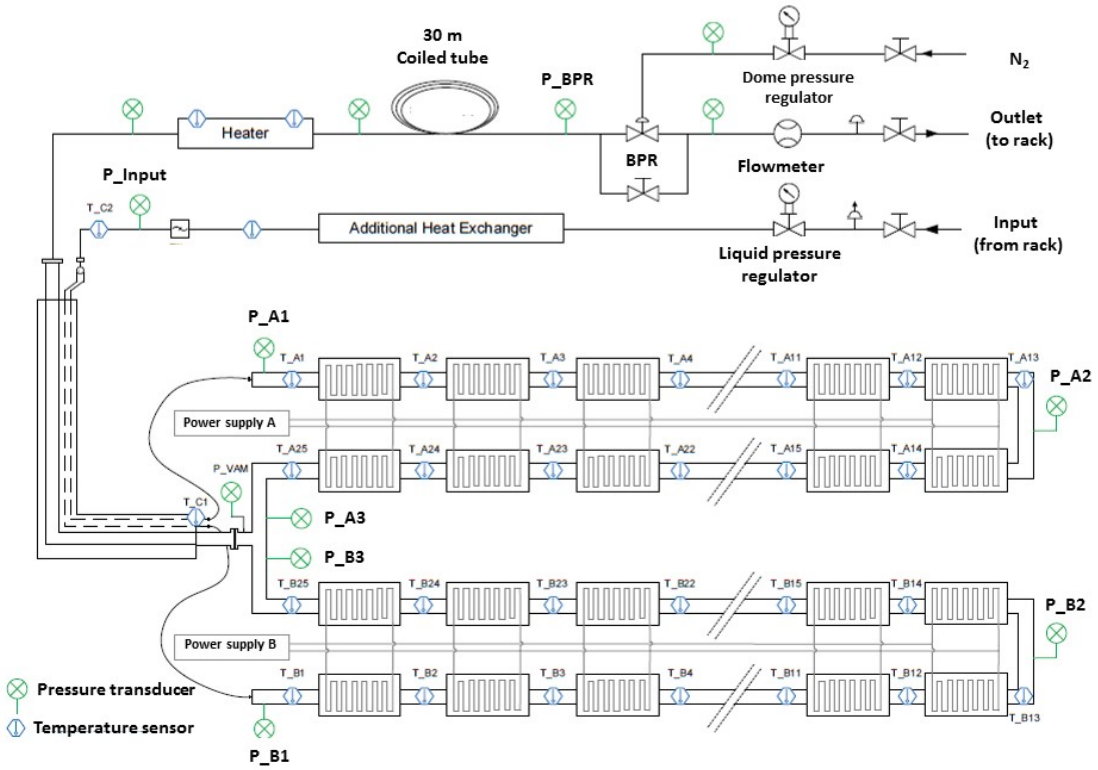

Figure 3. Thermal test structure representing an SCT bi-stave cooling circuit (schematic), in which 48 silicon microstrip modules are emulated by ceramic heaters.

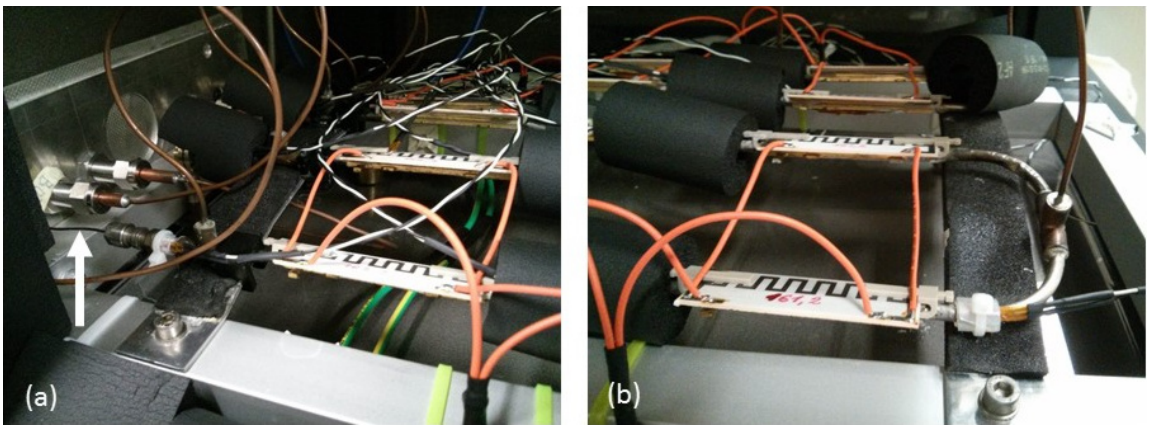

Figure 4. Views of the SCT bi-stave thermal test structure showing ceramic heaters and their attachment blocks: (a) injection and exhaust end showing a capillary (arrowed: the larger tubes connect to electronic pressure transducers): (b) 180 "turn around" at the opposite end, with temperature sensors and tube allowing mid-point pressure measurement.

2015 JINST 10 P03027

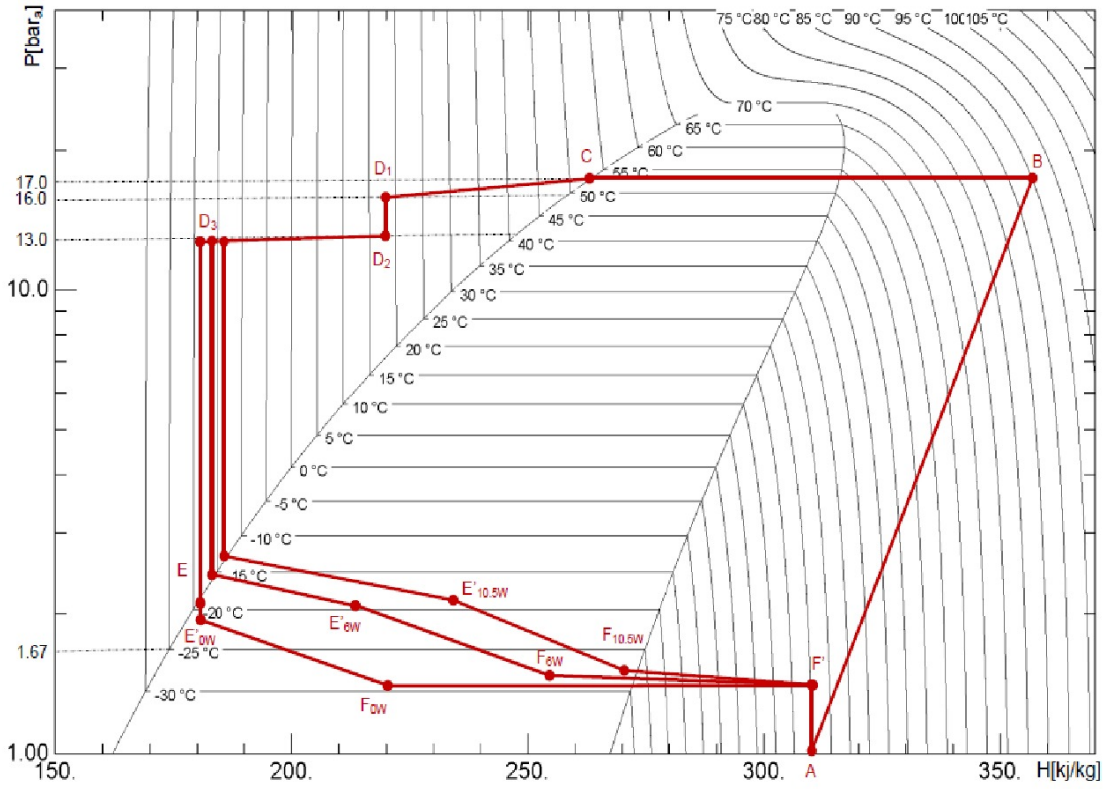

Figure 5. Thermodynamic cycles on a pressure-enthalpy diagram for the evaporative cooling system operating with pure C_3F_8: at total power loads of 0 W, 288 W & 504 W in the SCT bi-stave thermal test structure [6].

sub-cooling heat exchanger against temperature variations in the test building. The injected flow represented 120% of that needed to cool the structure at the maximum on-detector power load of 504 Watts.

Fluorocarbon refrigerant leaving the SCT test structure (containing a variable amount of unevaporated liquid, depending on the power dissipation in the preceding test structure) was evaporated in a downstream electrical heater, which also raised the exhaust vapour temperature to 20°C (maintaining the same safety margin above the expected cavern dew point of 12°C) as in the installed detector, for return to the blend machine compressor.

The evaporation pressure in the test structure was set by the BPR, located downstream of the heater, following $\sim$ 30 m of uninsulated copper pipe, as in the installed system [6].

The achievable thermodynamic cycles, based on measurements made in the test structure dissipating 0 W, 288 W and 504 W in total; respectively equivalent to 0 W, 6 W and 10.5 W per module are shown in figure 5. Table 2 details the various state transitions.

It can be seen from figure 5 — even with injection at around -15°C — that the exhaust pressure drop **E' FF'** exceeded the specification [1], with the greatest effect coming from the pressure drop in the exhaust heat exchanger (segment **E'F**). This pressure drop raised the evaporation temperature

2015 JINST 10 P03027

Table 2. Transition points on the enthalpy-pressure diagram of figure 5 for operation with C_3F_8 in the test structure.

Transition	Physical State and location
A→B	C_3F_8 vapour compressed from 1 to 17 bar_{abs}, heated to 90°C in a 2-stage compressor.
B→C	C_3F_8 vapour condensed inside the condenser at 53°C and delivered to a storage tank.
C→D_1	C_3F_8 liquid cooled in the storage tank and along its delivery path to the liquid supply pressure regulator.
$D_1 \rightarrow D_2$	Pressure drop from 16 to 13 bar $_{abs}$ across the liquid supply pressure regulator and along the liquid delivery tubing to the SCT detector.
$D_2 \rightarrow D_3$	Liquid sub-cooling in the local liquid supply heat exchanger by counter-flow of remaining liquid/cold vapour in the exhaust line. Note: the sub-cooling temperature (point D_3) depends on total heat load in the test structure.
$D_3 \rightarrow E$	Isenthalpic pressure drop across the throttling element (capillary).
E→E'	Refrigerant evaporation, removing heat from the test structure for power loads equivalent to 0 W, 6 W & 10.5 W/module, respectively.
E'→F	Pressure drop and enthalpy use in the local heat exchanger to sub-cool the incoming liquid in segment $D_2 \rightarrow D_3$. Note the different positions for 0 W, 6 W & 10.5 W/module.
F→F'	Remaining liquid evaporated in the exhaust electric heater and vapour warmed to 20°C. Note the different starting positions for 0 W, 6 W & 10.5 W/module due to different amounts of excess liquid arriving at the heater input.
F'→A	Pressure drop in superheated vapour measured in the exhaust line from the heater to the compressor input, including the pressure drop across the BPR.

— and with it the module operating temperature — by more than 10°C (13°C) from the -25°C design figure when the bi-stave was operated at power dissipations of equivalent to 6 W and 10.5 W dissipation per module respectively. The temperature gradient along the on-detector evaporator **EE'** also exceeded the SCT specification of 5°C [7].

The effects of these pressure drops are also manifested in differences between the maximum evaporation temperatures measured on the tube wall and that expected from the C_3F_8 saturated vapour temperature corresponding to the pressure at the BPR, as illustrated in figure 6.

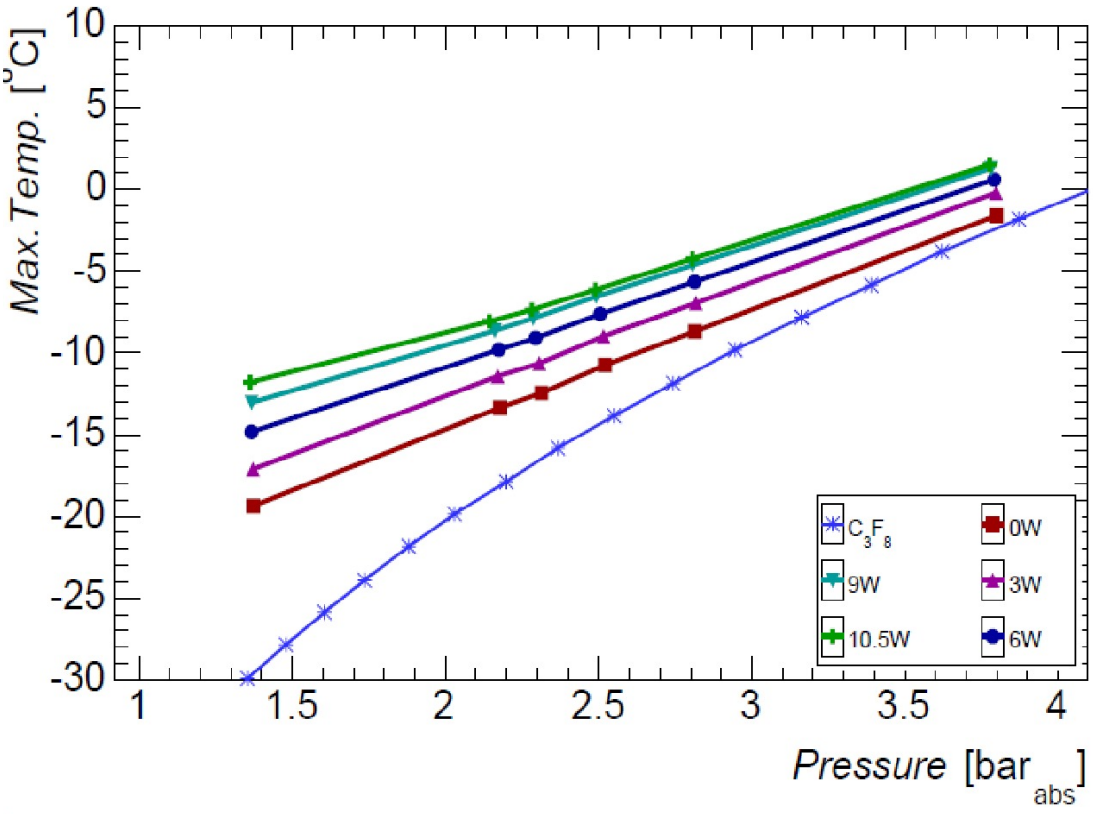

Figure 6. Maximum temperature on the cooling tubes of a representative SCT barrel bi-stave test setup, *vs.* pressure at the input of a back pressure regulator installed 30 m downstream, for different applied power (per module: 48 modules total: [6]). Pure C_3F_8 coolant, input liquid pressure 13 bar_{abs}, mass flow 12.7 $\pm$ 0.3 $g.s^{-1}$. Temperature (backpressure) measurement precision $\pm$ 0.35°C ($\pm$ 5 mbar). C_3F_8 saturated vapour pressure curve from NIST-REFPROP [8] shown for comparison.

The abscissa of figure 6 is the pressure measured at the input of the BPR ($\mathbf{P}_{BPR}$ in figure 3) around 30 metres downstream of the heater. The BPR is 'dome-loaded': a pneumatic command signal in the range 1–4 bar_{abs} applied to its dome sets the pressure immediately upstream of the device, to which the evaporation pressure in the on-detector cooling tube is referenced via the incremental pressure drop in the preceding exhaust tubing, heater and heat exchanger (figure 1). Remote analogue pneumatic signals have been chosen for use in the high radiation zones of ATLAS due to the simultaneous presence of high magnetic fields.

From figure 6 it can be seen that at P_{BPR} = 1.35 bar_{abs} the maximum temperatures measured along the on-detector cooling tube were -11.8 °C, -15°C and -17.5°C for total power dissipations equivalent to 10.5 W, 6 W and 3 W per module. These temperatures respectively correspond to local ("on-detector" cooling tube) evaporation pressures of 2.75, 2.47 and 2.25 bar_{abs}. The differences between these pressures and the BPR input pressure of 1.35 bar_{abs} manifest the effect of pressure drop in the exhaust tubing linking the emulated bi-stave to the BPR. The increase is particularly pronounced at lower system pressures where the C_3F_8 saturated vapour density is lower (resulting

2015 JINST 10 P03027

in a higher liquid → vapour expansion ratio and a consequently higher exhaust vapour volume flow). It can further be seen from figure 6 that an on-detector evaporation temperature of -15 °C cannot be reached at total dissipations equivalent to 9 W and 10.5 W per module.

The consequent perceived risk of leakage power-induced thermal runaway in SCT silicon sensors after extended operation at LHC motivated an investigation into the possible reduction of evaporation temperature through the circulation of blends of C_2F_6 and C_3F_8 within the existing SCT on-detector cooling tubes. This would in turn reduce the temperature-dependent leakage power and extend the safety margin against thermal runaway.

At the time of writing this paper updated LHC luminosity projections suggest that leakage power will be lower than previously foreseen, with the consequence that pure C_3F_8 is likely to be sufficient. Nevertheless, the ability to use blends to lower the evaporation temperature provides a vital backup solution should requirements or projections change in the future.

1.4 C_2F_6/C_3F_8 blends for lower evaporating temperatures in existing cooling structures

Although from figure 6 it can be seen that an evaporation temperature of -15 °C is not achievable using pure C_3F_8 in an SCT bi-stave at the highest module power levels, calculations with the NIST-REFPROP package [8] suggested that evaporation temperatures of -15°C and below would be reachable by blending C_3F_8 with a more volatile component of similar (radiation resistant, non-flammable and dielectric) chemical structure. This possibility stimulated the study reported in this paper.

Among the saturated fluorocarbons of structure $C_nF_{(2n+2)}$, *hexafluoro-ethane* (C_2F_6; mw = 138) is the nearest neighbouring fluid of increased volatility. The addition of sufficient C_2F_6 in a binary blend would be expected to reduce the evaporation temperature for the same evaporation pressure (or increase the evaporation pressure for the same evaporation temperature), allowing sufficient margin to overcome the pressure drops seen with pure C_3F_8.

In contrast to the case of pure C_3F_8, evaporation and condensation in C_2F_6/C_3F_8 blends are not simultaneously isothermal and isobaric. Due to their similar chemical structure C_2F_6/C_3F_8 blends can be considered as zeotropic mixtures manifesting "temperature glide" when evaporating and condensing. Temperature glide is illustrated in figure 7 for a molar blend of 85% C_3F_8/ 15% C_2F_6, while table 3 compares the Saturated Liquid Pressure (S.L.P) and Saturated Vapour Pressure (S.V.P) for evaporation at temperatures of -25°C and -15°C in pure C_3F_8 and a variety of C_2F_6/C_3F_8 blends of thermodynamic interest. Also shown in table 3 is the maximum temperature glide assuming all the available enthalpy of evaporation is used. In practice, not all the enthalpy is available for use in the on-detector evaporator (cooling tube): the liquid sub-cooling temperature may be warmer than the evaporation temperature, while evaporation enthalpy may be shared between the on-detector evaporator and a downstream exhaust heat exchanger and heater (figure 1). Taking an example from figure 7; the use of only half of the $\sim$ 110 $kJkg^{-1}$ of available enthalpy (illustrated in figure 7 using a violet band) in the on-detector cooling channel at an evaporation pressure of 1.94 bar_{abs} and an injection temperature of -15°C would result in a temperature rise of $\sim$ 6°C (illustrated in red) from the injection point to the exit of the on-detector cooling channel. This temperature glide effect would be partially opposed however by the dynamic temperature gradient due to evaporation pressure drop with distance from the input of the channel. This dynamic

2015 JINST 10 P03027

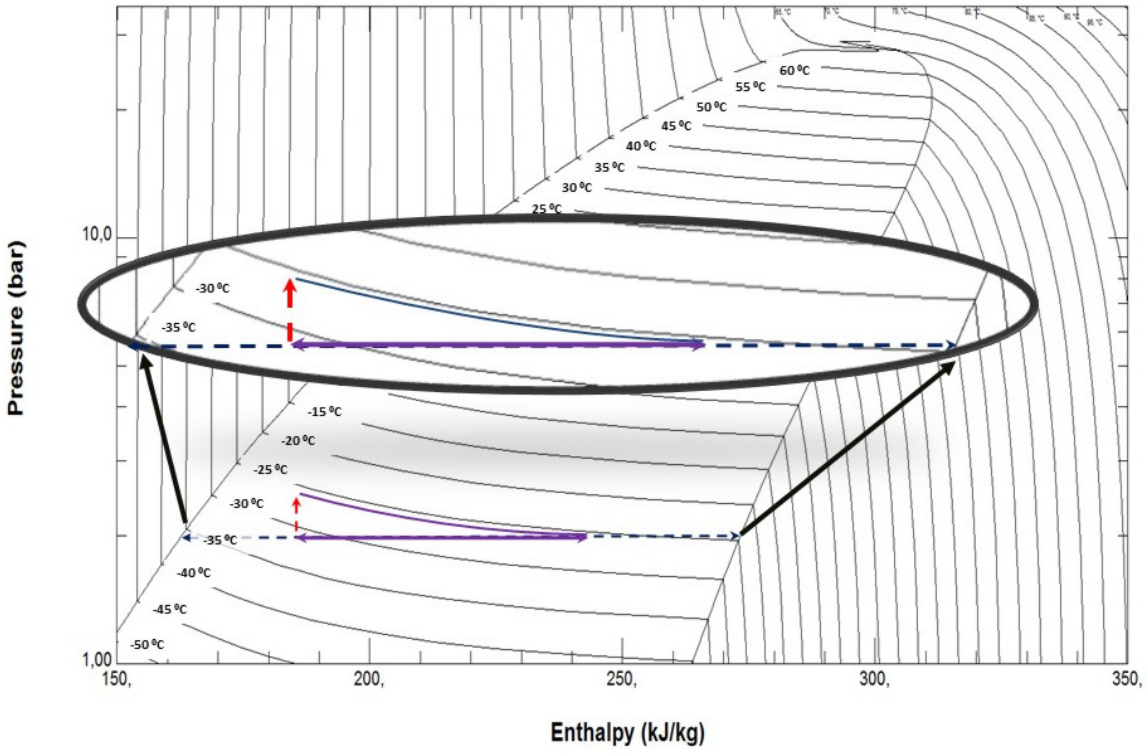

Figure 7. Pressure-enthalpy diagram for a molar blend of 85% C_3F_8/15% C_2F_6 (from NIST-REFPROP [8]). The curving evaporation isotherms illustrate the naturally anisobaric nature of the phase change. The use of half the available enthalpy (shown in violet in inset) at an evaporation pressure of 1.94 bar_{abs} with injection at -15°C would result in a temperature rise ("glide") of $\sim$ 6°C (shown in red in inset).

Table 3. Evaporation characteristics of several C_2F_6/C_3F_8 molar blends of interest. Saturated liquid and vapour pressures for evaporation at -25°C and -15°C, with maximum temperature glide for evaporation, referenced to the saturated vapour pressure. Calculations made using the NIST-REFPROP package [8].

Molar conc. C_2F_6	Saturated Liquid (Vapour) pressure (bar_{abs}): evaporation at -25°C	Maximum Temperature glide (evaporation at *S.V.P.*)	Saturated Liquid (Vapour) pressure (bar_{abs}): evaporation at -15°C	Maximum Temperature glide (evaporation at *S.V.P.*)	Sound velocity (ms^{-1}) in superheated vapour (20°C, 1 bar_{abs})
0	1.67 (1.67)	0°C; 1.67 bar_{abs}	2.47 (2.47)	0°C; 2.47 bar_{abs}	115.0
5	2.12 (1.76)	5.0°C; 1.76 bar_{abs}	3.03 (2.58)	4.6°C; 2.58 bar_{abs}	115.9
10	2.56 (1.84)	8.8°C; 1.84 bar_{abs}	3.59 (2.71)	8.2°C; 2.71 bar_{abs}	116.8
15	2.96 (1.94)	11.7°C; 1.94 bar_{abs}	4.11 (2.85)	11.0°C; 2.85 bar_{abs}	117.7
20	3.33 (2.05)	13.8°C; 2.05 bar_{abs}	4.61 (3.01)	13.1°C; 3.01 bar_{abs}	118.7
25	3.72 (2.16)	15.4°C; 2.16 bar_{abs}	5.08 (3.18)	14.6°C; 3.18 bar_{abs}	119.7
30	4.06 (2.30)	16.4°C; 2.30 bar_{abs}	5.57 (3.37)	15.6°C; 3.37 bar_{abs}	120.7

temperature gradient is readily observable in the evaporation of a pure coolant like C_3F_8 — the exhaust end of an on-detector evaporator being colder than the input.

2015 JINST 10 P03027

In operation with C_2F_6/C_3F_8 blends it will be necessary to monitor the molar mixture ratio and if necessary to adjust it with the addition of either component. The C_2F_6/C_3F_8 mixing station and recirculator is discussed in section 2.1, while the protocol used to create C_2F_6/C_3F_8 molar blends is discussed in appendix A.

The C_2F_6/C_3F_8 molar ratio is best monitored through measurement of sound velocity in the superheated (single phase) vapour state. In table 3 the sound velocities at 20°C, 1 bar_{abs} were calculated for various C_2F_6/C_3F_8 blends using the NIST-REFPROP package [8]. The custom ultrasonic instrument developed for simultaneous on-line blend composition and vapour flow measurement [9] is discussed in appendix B.

Results from thermal studies with pure C_3F_8 and in C_2F_6/C_3F_8 blends in a test structure representing an SCT barrel bi-stave are presented in section 3.

2 The blend recirculation machine and cooling circuit

2.1 The blend recirculation machine

Figure 8 illustrates the custom-built fluorocarbon blend recirculation machine, while figure 9 shows the schematic of the blend machine local components. The machine can be used to create and circulate molar blends of C_3F_8 and C_2F_6.

The principal elements of the blend recirculator are:

- a three-cylinder, single stage oil-less compressor[9] operating with a typical aspiration pressure of 1000 $mbar_{abs}$ and an output pressure of 9 bar_{abs};
- a high pressure condenser/reservoir tank cooled to operate in the range (-30 → 20°C); by a refrigerator operating with R404A refrigerant;
- a liquid pressure booster pump[10] located around 2.5 m below the condenser, which adds around 7 bar to the pressure of the liquid leaving the condenser;
- weighing platforms for the condenser/reservoir tank and the C_2F_6 and C_3F_8 cylinders. These platforms allow molar blends of C_3F_8 and C_2F_6 to be created by mass addition in the liquid phase according to the protocol discussed in appendix A;
- an ultrasonic vapour mixture analysis instrument for measurement of the molar C_2F_6 and C_3F_8 concentrations in superheated vapour. The instrument is discussed in appendix B.

The blend machine operation is highly automated: the main parameters of the system can be set and monitored remotely using the CERN UNICOS [10] distributed control system environment.

In the thermal studies with C_2F_6/C_3F_8 blends it was intended to reproduce as far as possible the as-installed liquid delivery and vapour return configuration. However since no two-stage compressor could be spared for integration into the blend machine a booster pump was used to raise the liquid pressure to around 16 bar_{abs}: a pressure sufficient to deliver the liquid via the 50 m of tubing linking the blend recirculator and the thermal test stand. The compressor output pressure was

[9] Haug Model WTEGX80 LM-L, maximum nominal output (minimum nominal aspiration) pressures of 11(0.8) bar_{abs} flow rate 17m^3hr^{-1} C_3F_8 at P_{in} = 1.0 bar_{abs}, P_{out} = 7 bar_{abs}.

[10] "V-modular" series two-stage sliding vane pump Model 01/2S: nominal maximum liquid flow 75 lhr^{-1} at 15 bar_{abs} output pressure: M3 Pumps s.r.l., Via dell'Artigianato 120, 45015 Corbola, Italy.

2015 JINST 10 P03027

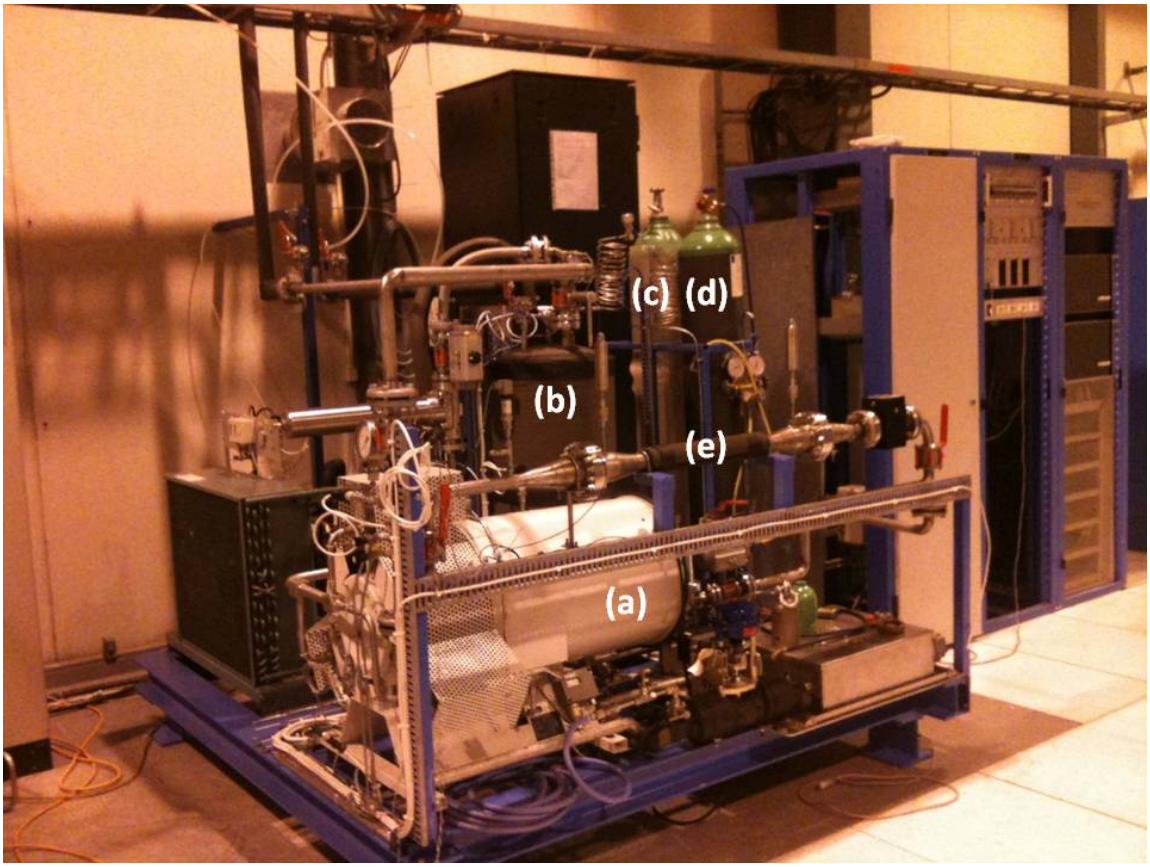

Figure 8. Photograph of the blend recirculation machine, illustrating the compressor (a), condenser (b), the C_2F_6 and C_3F_8 cylinders (c,d), together with the custom-built ultrasonic gas mixture analyser (e) used for confirmation of C_2F_6/C_3F_8 blends set up in the machine.

limited to 9 bar_{abs}; around 2 bar lower than its maximum pressure in order to reduce mechanical strain. Fluorocarbon vapour (either pure C_3F_8 or C_2F_6/C_3F_8 blend) was condensed at this pressure. Liquid fluorocarbon leaving the condenser at 9 bar_{abs} descended around 2.5 m to the liquid booster pump, which added around 7 bar relative to the output pressure of the condenser. The liquid descending to the pump passed through a heat exchanger which was counter-cooled with a water/glycol mix, leaving with a temperature in the range 15–17°C. Together with the hydrostatic column of 2.5 m (plus the liquid height in the condenser) this ensured that the pump was always kept primed to avoid vapour-induced cavitation. The 50 m interlink tubing was insulated with 25 mm of Armaflex® foam and passed through an air-conditioned zone.

2.2 Examples of thermodynamic cycles in operation with C_3F_8 and C_2F_6/C_3F_8 blends

Figure 10 illustrates the measured thermodynamic cycle on an enthalpy-pressure diagram for the blend recirculator operating with pure C_3F_8, the reference with which all thermal studies with blends are later compared. Figure 11 illustrates the measured thermodynamic cycle on an enthalpy-pressure diagram for the blend recirculator operating with a molar blend of 75% C_3F_8/25% C_2F_6.

2015 JINST 10 P03027

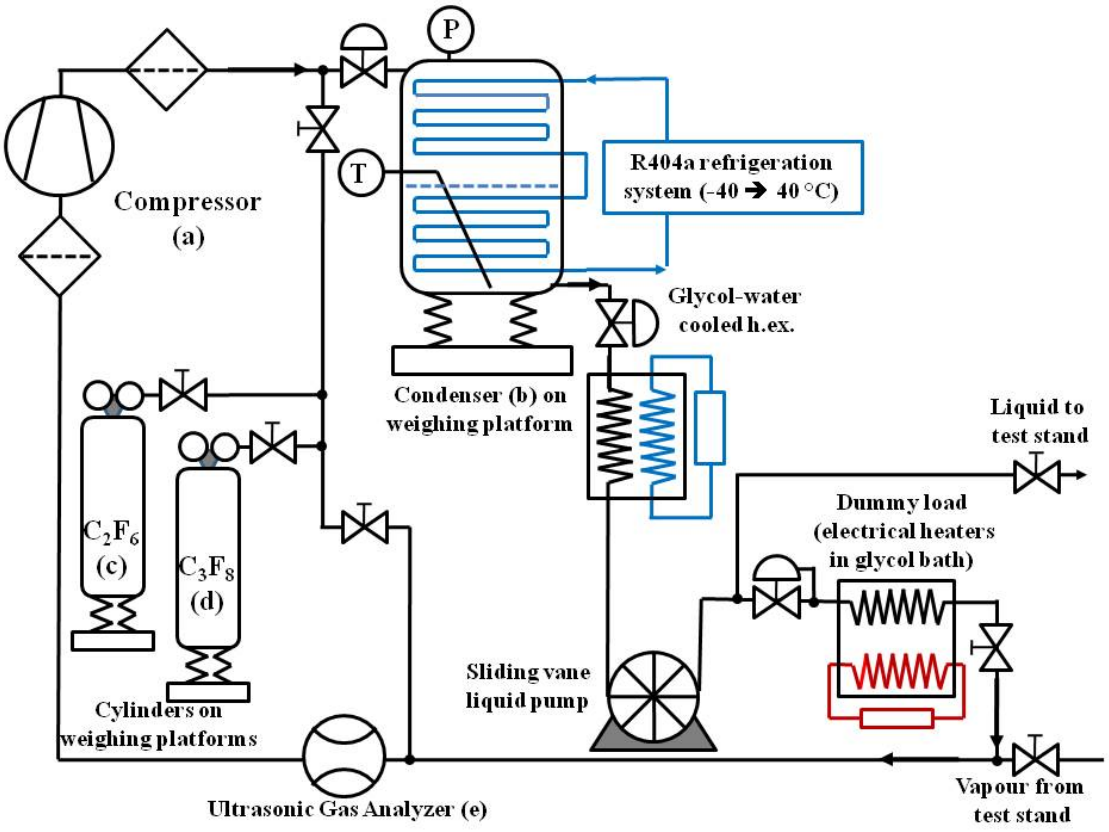

Figure 9. Schematic of the blend recirculation machine local components.

Systematic differences due to the constraints of the blend recirculation machine can be seen relative to the thermodynamic cycle of figure 5;

- the lower compression available in the single stage compressor (segment **AB**);
- the increase in liquid pressure from the booster pump (segment $\mathbf{CD}_1$).

Some differences between the thermodynamics of figures 10 and 11 are also readily apparent:

- in the molar blend of 75% C_3F_8/25% C_2F_6 the maximum evaporation temperature 'glide' (traversal of isotherms along the on-detector evaporation segment **EE'**) of around 4°C is seen for zero heat load;
- in the same blend the condensation pressure is defined by the 9 bar_{abs} output pressure of the compressor, causing the blend to condense over the 14°C temperature 'glide' between 16°C (incoming vapour) and 2°C (bulk liquid) in the volume above the liquid in the condenser/reservoir tank.
- the fluid starts boiling in the capillary.

Table 4 summarises and discusses the transition points on the thermodynamic cycles shown in figures 10 and 11 for circulation of pure C_3F_8 and the molar blend of 75% C_3F_8/25% C_2F_6.

2015 JINST 10 P03027

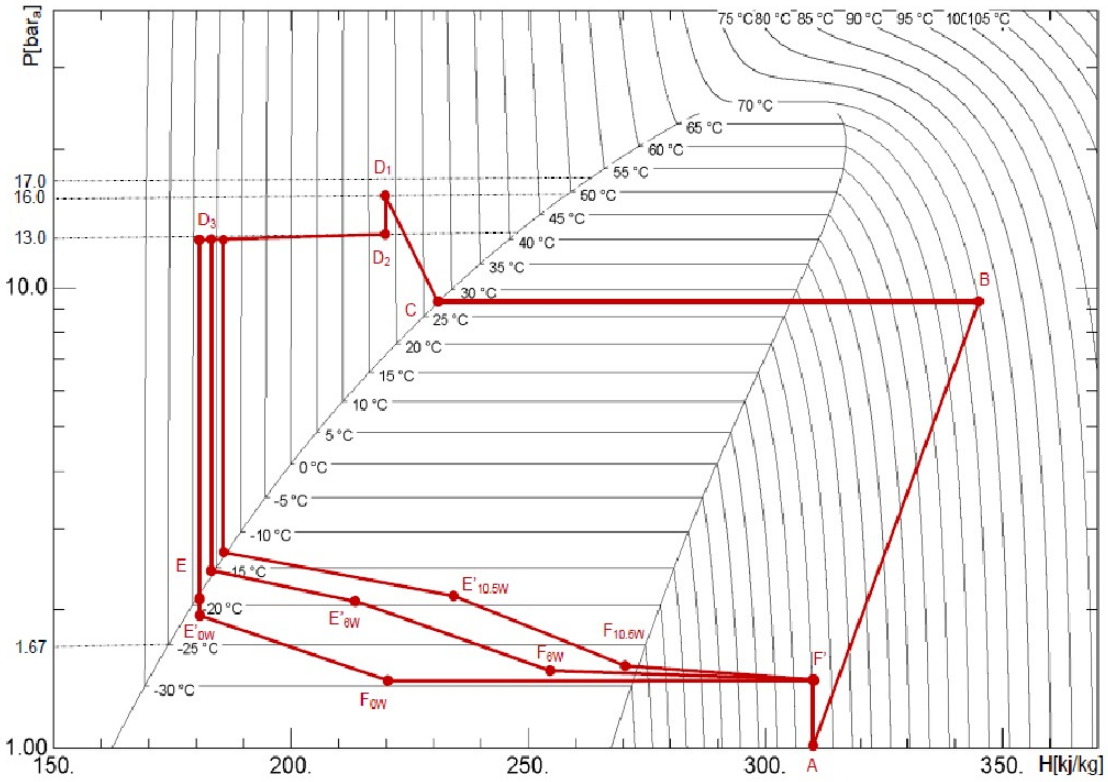

Figure 10. Thermodynamic cycle on a enthalpy-pressure diagram for the blend recirculator operating with pure C_3F_8 at power loads of 0, 288 & 504 W in the emulated SCT bi-stave; backpressure set to 1.2 bar_{abs}.

3 Comparison of cooling performance in C_3F_8 and C_2F_6/C_3F_8 blends

Thermal profiles were measured along the cooling tubes (staves) of the SCT test structure of figure 3, at power settings of 0 W, 3 W, 6 W, 9 W and 10.5 W per dummy module. The two identically-powered staves of 24 thermal emulator modules shared a common output: the exhaust pressure drop was therefore comparable with that of an operational SCT barrel bi-stave.

These measurements were repeated for nominal C_2F_6 molar concentrations of 0%, 1%, 3%, 5%, 10%, 20% and 25% in the C_2F_6/C_3F_8 blend. These concentrations were "targets" for the blending protocol described in appendix A: the achieved concentrations were verified to a precision of $\pm$ 0.3% in the ultrasonic analyser discussed in appendix B.

Figure 12 illustrates the complete temperature profile along one of the staves, read out by 25 sensors attached to the cooling tubes between the dummy modules. The upper plots show the temperature profiles at the different module power dissipations for pure C_3F_8 coolant (solid lines) while the lower plots show temperature profiles at the same power dissipations for a blend containing 25%C_2F_6/75%C_3F_8 (dashed lines). All data in figure 12 correspond to a back pressure (P_{BPR}) of 1.2 bar_{abs}. Figure 13 illustrates the corresponding temperature profiles at the same power settings for P_{BPR} = 2 bar_{abs}. The liquid pressure at the capillary input was 13 bar_{abs} for both backpressures.

2015 JINST 10 P03027

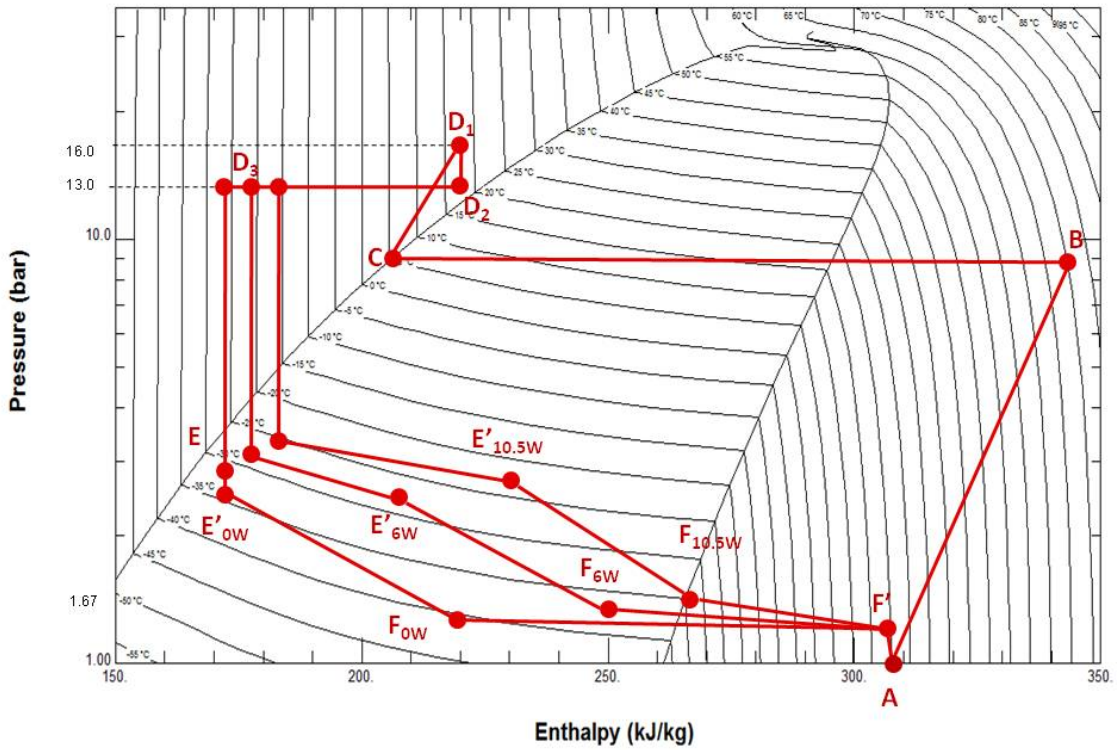

Figure 11. Thermodynamic cycle on an enthalpy-pressure diagram for the blend recirculator operating with a molar blend of 75% C_3F_8/ 25% C_2F_6 at total power loads of 0, 288 & 504 W in the emulated SCT bi-stave; backpressure 1.2 bar_{abs}.

It can be seen that the temperature profile along the stave in the 25%C_2F_6/75%C_3F_8 blend increases toward the exit, in contrast to the reduction generally seen in pure C_3F_8. This effect is the result of the opposing effects of temperature glide and dynamic temperature gradient along the evaporator and is most apparent when almost the full enthalpy is used in the stave at a power of 10.5 W per module. Nevertheless at this power the maximum temperature on the tube remains no higher than -21°C (-15°C) with P_{BPR} = 1.2 bar_{abs} (2 bar_{abs}).

Figure 14 illustrates the maximum temperature seen on the tubes of the emulated SCT bi-stave as a function of the ultrasonically-verified molar concentration of C_2F_6 in the blend, for three different power (per module) levels, with P_{BPR} = 1.2bar_{abs}. As expected, the addition of the more volatile C_2F_6 component reduced the evaporation temperature on the cooling tubes under the same operational "envelope"; the same liquid supply and exhaust backpressures. The improvements for 0 W, 6 W and 10.5W per module are respectively characterised by gradients of approximately -0.50, -0.45 & -0.37°C.%$[C_2F_6]^{-1}$.

The addition of 25% C_2F_6 was found to reduce the maximum evaporation temperature on the cooling tubes from -12°C (-15°C) at a dissipation of 10.5 (6) Watts per module to -21°C (-25°C) respectively when operating at the same backpressure.

Figure 15 compares the maximum temperature seen on the tubes of the emulated SCT bi-stave with pure C_3F_8 to that seen in a blend containing 25% C_2F_6, at P_{BPR} values of 1.20, 2.26, 2.40, 2.60 and 2.78 bar_{abs}.

2015 JINST 10 P03027

Table 4. Transition points on the enthalpy-pressure diagram of figures 10 & 11 for blend recirculator operation with an emulated SCT barrel bi-stave operating with pure C_3F_8 and a molar blend of 75%C_3F_8/25%C_2F_6.

Transition	Physical State and location
A→B	Refrigerant vapour is compressed from 1 bar_{abs} to 9 bar_{abs} and heated to 70°C by a single stage compressor.
B→C	Refrigerant vapour condenses inside the condenser/storage tank (at 27°C for pure C_3F_8 and over the range 17°C → 5°C for 25% C_2F_6/75% C_3F_8).
C→D_1	Refrigerant in liquid state from the condenser/storage tank is sub-cooled before the liquid booster pump to a temperature of 17°C, and is raised in pressure to 16 bar abs by the pump. In the case of 25% C_2F_6/75% C_3F_8 the refrigerant is warmed to 17°C.
D_1 → D_2	Pressure drop from 16 bar_{abs} to 13 bar $_{abs}$ across the liquid supply pressure regulator and liquid delivery tubing to the emulated SCT bi-stave.
D_2 → D_3	Liquid sub-cooling in the local liquid supply heat exchanger by counter-flow of remaining liquid/cold vapour in the exhaust line (to -15°C for pure C_3F_8 and -25°C for 25% C_2F_6/75% C_3F_8) Note: exact sub-cooling temperature (point D_3) depends on the total heat load in the emulated SCT bi-stave.
D_3 → E	Isenthalpic pressure drop across the capillary.
E→E'	Refrigerant evaporation removing heat from the emulated SCT bi-stave for power loads equivalent to 0 W, 6 W & 10.5 W/module.
E'→F	Pressure drop and enthalpy use in the local heat exchanger to sub-cool the incoming liquid in segment D_2 →D_3. Note the different positions for 0 W, 6 W & 10.5 W/module.
F→F'	Remaining liquid evaporated in the exhaust electric heater and vapour warmed to 20°C. Note the different starting positions for 0 W, 6 W & 10.5 W/module due to different amounts of unevaporated liquid leaving the emulated SCT bi-stave.
F'→A	Pressure drop in superheated vapour measured in the exhaust line from the heater to the compressor input, including the pressure drop across the BPR.

2015 JINST 10 P03027

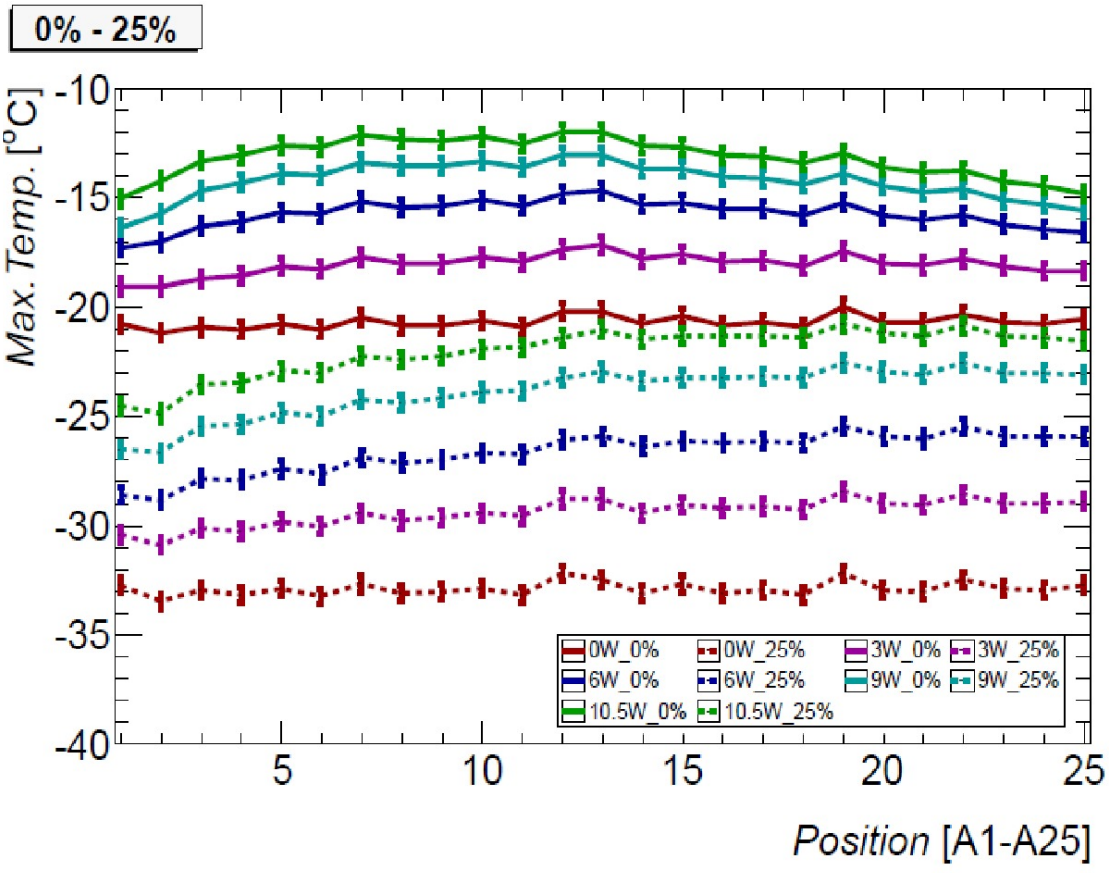

Figure 12. Comparison of the temperature profile along an SCT Barrel staves in pure C_3F_8 (solid lines) and with 25%C_2F_6/75%C_3F_8 blend (dashed lines) [6], at 1.2bar$_{abs}$ backpressure. Temperature measurement precision: $\pm$ 0.35°C.

A comparison of the left and right hand plots of figure 15 illustrates again that 25% C_2F_6 in a C_2F_6/C_3F_8 blend is capable of reducing the maximum temperature on the cooling tubes by 9°C in operation at the highest power level of 10.5 W per module.

Figure 15 further illustrates that in such a blend an evaporation temperature of -15°C is achievable everywhere on the structure for operation at $P_{BPR} \leqslant 2.38$ bar$_{abs}$. This cooling tube temperature would allow a safety factor of two in heat dissipation against thermal runaway in SCT silicon module substrates after 10 years of LHC operation, as outlined in section 1.1.

Figure 16 compares the maximum temperature seen in operation with pure C_3F_8 to that seen in a blend containing 25% C_2F_6 for the corresponding pressures sensed at the 180° half way points (figure 3). It can be seen that the temperature-pressure profiles for the different power levels become almost collinear with the C_3F_8 saturation line. In the 25%C_2F_6/75%C_3F_8 blend all the temperature-pressure profiles fall within the zone delineated by the saturated liquid pressure (lower) and saturated vapour pressure (upper) curves. As the power increases the temperature-pressure profiles migrate progressively toward the saturated vapour line as more vapour is produced by evaporation, and toward higher pressures as the dynamic pressure drop increases.

2015 JINST 10 P03027

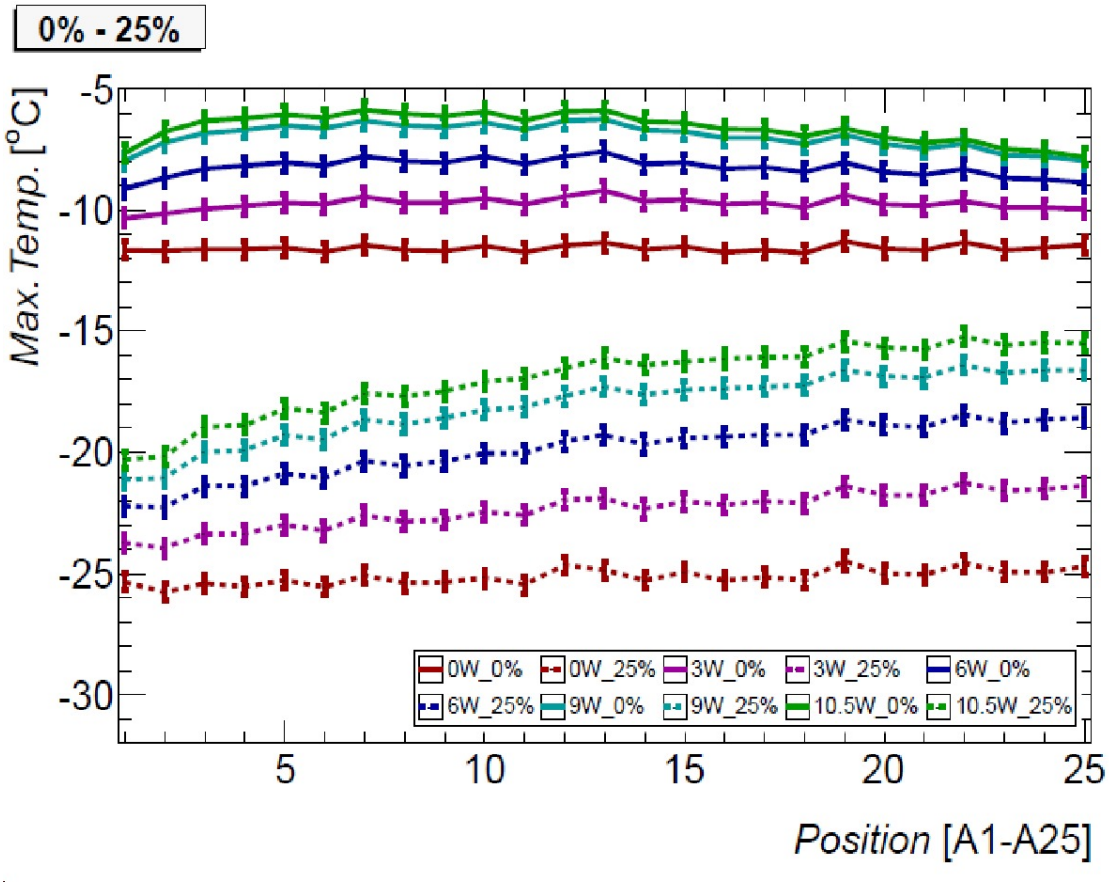

Figure 13. Comparison of the temperature profile along an SCT Barrel staves in pure C_3F_8 (solid lines) and with 25%C_2F_6/ 75%C_3F_8 blend (dashed lines) [6], at 2bar$_{abs}$ backpressure. Temperature measurement precision: $\pm$ 0.35°C.

Figure 17 illustrates the difference in maximum temperature seen on the tubes of the emulated SCT bi-stave between cooling with pure C_3F_8 and a blend containing 25%C_2F_6/75%C_3F_8, for five different power (per module) levels. In each case the pressure upstream of the capillary is 13bar$_{abs}$ while P_{BPR} varies between 1.2 and 3 bar$_{abs}$. It can be seen that a reduction in operating temperature of at least 8.5°C is possible for all power levels in a blend containing 25% C_2F_6.

4 Conclusion

We have constructed a custom thermodynamic recirculator that has been used for investigations of the cooling capabilities of C_2F_6/C_3F_8 blends with molar admixtures of up to 25% C_2F_6. The cooling performance of these blends was studied in a representative test setup of an ATLAS barrel SCT bi-stave containing 48 thermal emulator modules. The test structure incorporated an exhaust heat exchanger, an electric heater, backpressure regulator and intervening tubing identical to those used in the installed SCT system. Fluorocarbon blend molar concentrations were verified in the superheated vapour phase using an ultrasonic instrument with a typical resolution of $\pm$ 0.3%.

2015 JINST 10 P03027

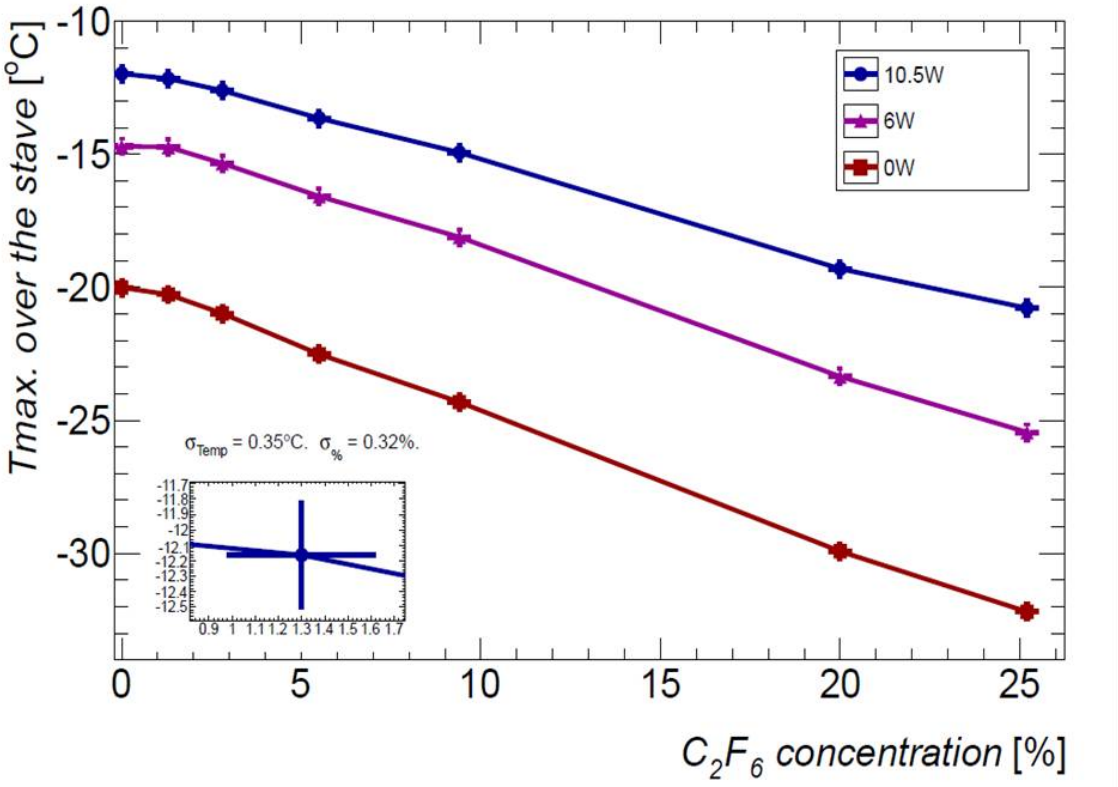

Figure 14. Maximum temperature on a tube of the SCT bistave *vs* C_2F_6 concentration in the blend, for three different power (per module) levels [6]. In each case the input pressure is 13bar$_{abs}$ upstream of the capillary and the back pressure is 1.2bar$_{abs}$. Temperature (mixture) measurement precision: $\pm$ 0.35°C ($\pm$ 0.3%: appendix B).

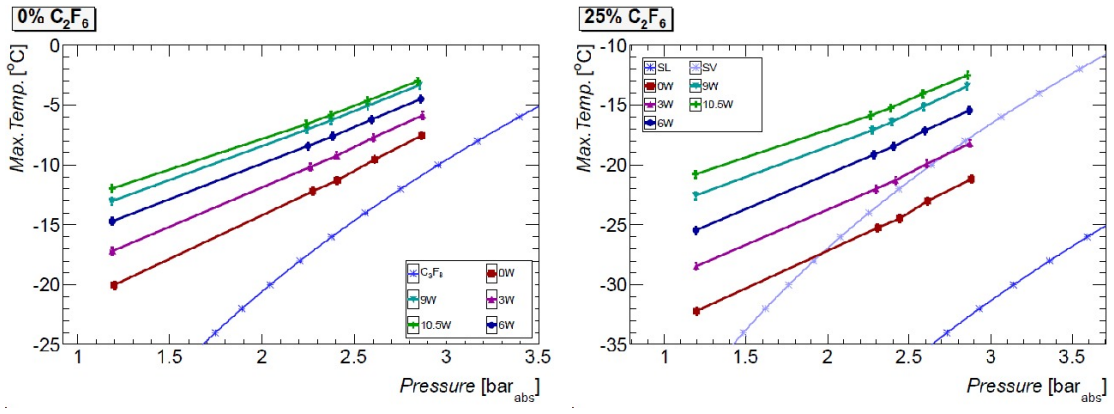

Figure 15. Maximum evaporation temperature on the cooling tubes between dummy modules in an SCT barrel bi-stave evaporator as a function of the pressure measured at the input of the back pressure regulator [6], for different applied detector power (per module: 48 modules total). Temperature (pressure) measurement precision: $\pm$ 0.35°C ($\pm$ 15 mbar) *Left plot*: pure C_3F_8, with C_3F_8 saturation curve shown for comparison. *Right plot*: 25%C_2F_6/75%C_3F_8, with saturated vapour (upper) and saturated liquid (lower) curves.

2015 JINST 10 P03027

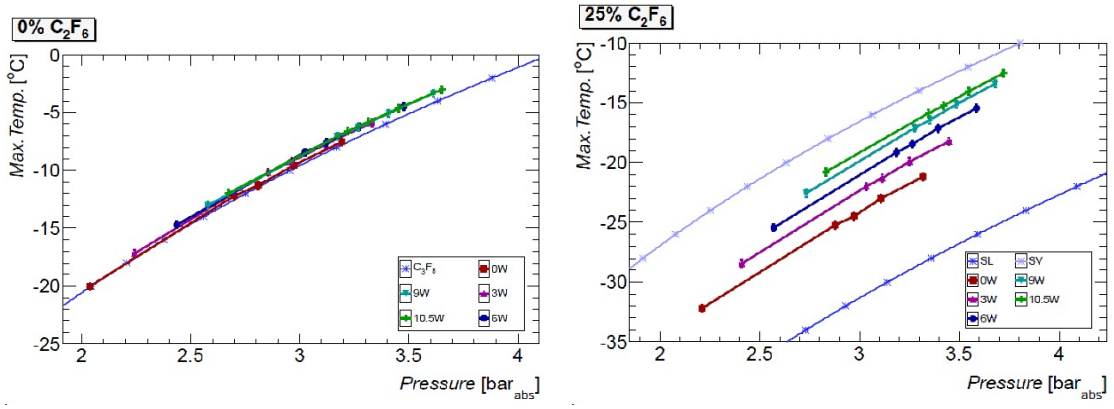

Figure 16. Maximum evaporation temperature on the cooling tubes between dummy modules in an SCT barrel bi-stave evaporator as a function of the pressure measured at the half-way point between the two staves [6], for different applied detector power (per module: 48 modules total). Temperature (pressure) measurement precision: $\pm$ 0.35°C ($\pm$ 15 mbar) *Left plot*: pure C_3F_8, with C_3F_8 saturation curve shown for comparison. *Right plot*: 25%C_2F_6/75%C_3F_8, with saturated vapour (upper) and saturated liquid (lower) curves.

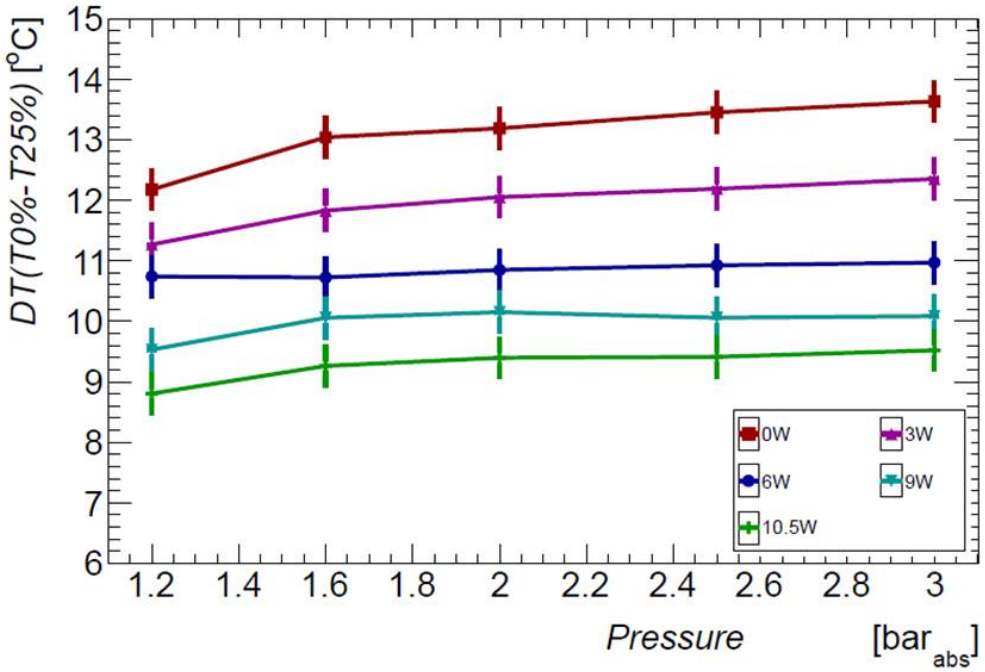

Figure 17. Reduction of maximum temperature on a tube of the SCT bistave *vs* pressure, by replacing pure C_3F_8 with a blend containing 25% C_2F_6. Data are shown for five different backpressures and power (per module) levels [6]. The pressure upstream of the capillary is 13bar_{abs}. Temperature measurement precision: $\pm$ 0.35°C.

2015 JINST 10 P03027

As expected, the addition of the more volatile C_2F_6 component reduced the evaporation temperature measured on the cooling tubes of the emulated SCT bi-stave. These improvements are characterized by gradients of approximately -0.50, -0.45 & -0.37°C.%$[C_2F_6]^{-1}$ respectively at power dissipations of 0, 6 and 10.5 W per emulated module. A new dedicated structure is being constructed for the measurement of absolute heat transfer coefficient in C_3F_8 and C_2F_6/C_3F_8 blends: measurements will be presented in a future work.

The addition of 25% C_2F_6 was found sufficient to reduce the evaporation temperature on the cooling tubes of a barrel SCT bi-stave from -12°C (-15°C) to -21°C (-25°C) at a dissipation of 10.5 (6) Watts per module, respectively in operation with an exhaust backpressure set to 1.2bar_{abs}. This temperature reduction would compensate for the pressure drops seen in inaccessible regions of the exhaust return tubing in operation with pure C_3F_8, and would be sufficient to allow the as-installed barrel SCT bi-staves to be operated for 10 years under demanding previously-foreseen LHC luminosity conditions, equivalent to an integrated luminosity of around 700 fb^{-1}.

While more recent LHC projections suggest an integrated luminosity of only 300–400 fb^{-1} over 10 years of operation up to the LHC 3^{rd} long shutdown ("3LS": currently proposed for 2023), it is clear that operation with a blend containing 25% C_2F_6 would provide a valuable safety net should the integrated luminosity accumulated before 3LS prove to exceed recent forecasts. Furthermore, a blend containing up to 25% C_2F_6 could be circulated in the existing ATLAS inner detector evaporative cooling system.

Acknowledgments

The authors wish to thank CERN and their home institutes for support for this project. University of Oklahoma participation was supported through DOE contract DE-FG02-04ER41305. A. Bitadze acknowledges support for his PhD research from the ATLAS inner detector group and the particle physics group of the University of Glasgow. R. Bates acknowledges support from the U.K. Science and Technology Facilities Council. M. Doubek, C. Rossi and V. Vacek acknowledge individual support and support for this project through the following grants in the Czech Republic: MSM grants FIS1401301D001 (LG13009) and SGS/FIS grant 1611320B001 of the Czech Technical University, Prague.

A The fluorocarbon blending protocol

In this work molar blends of C_3F_8 and C_2F_6 were created by mass addition in the liquid phase and verified by sound velocity measurements in the superheated vapour phase.

The blending procedure makes use of Raoult's law: the total vapour pressure above the liquid mixture depending on the vapour pressure of each component and the mole fraction of the component in the liquid mixture.

Once the components (i =A, B...) in the liquid mixture have reached equilibrium, the total vapour pressure p above the liquid mixture is given by:

$$p = p_A.x_A + p_B.x_B \ldots \tag{A.1}$$

2015 JINST 10 P03027

the individual vapour pressure for each component being:

$$p_i = p_i.x_i \tag{A.2}$$

where

$\boldsymbol{p}_i$ is the partial pressure of the component $\boldsymbol{i}$ in the mixture,
and $\boldsymbol{x}_i$ is the mole fraction of the component $\boldsymbol{i}$ in the liquid mixture.

In the blend machine, illustrated in figures 8 and 9, the condenser also serves as a liquid reservoir tank and is fitted with a dynamometer for weight measurements, while the cylinders containing the C_2F_6 and C_3F_8 constituents stand on weighing platforms, allowing a redundancy in mass transfer measurements.

A prerequisite for making or modifying a blend is that all the fluorocarbon liquid — and as much of the vapour as possible — is first recovered from the $\sim$ 60m external piping — back into the condenser to give a new mass baseline. This recovery is made using the compressor, with the liquid in the delivery line either being allowed to boil through the thermal test stand or (more quickly) through a thermal load bypass. In practice a small amount of vapour (at the minimum compressor aspiration pressure of 800 $mbar_{abs}$) remains in the liquid supply and vapour return piping after this operation. This must be evacuated before resuming circulation through the thermal test stand, to avoid changing the mixture of the new blend.

The number of moles per kilogram of C_2F_6 and C_3F_8 in a liquid mixture, given by the reciprocals of their molar masses of 0.138 and 0.188 kg, are respectively 7.25 and 5.32 $moles.kg^{-1}$.

The resulting C_2F_6 mole fraction, ${}_M\boldsymbol{C_2F_6}$,obtained through adding $\boldsymbol{X}$ kg liquid C_2F_6 and $\boldsymbol{Y}$ kg liquid C_3F_8 is given by:

$${}_MC_2F_6 = \frac{\frac{X}{0.138}}{\frac{X}{0.138} + \frac{Y}{0.188}} \tag{A.3}$$

To achieve a blend having desired molar C_2F_6 & C_3F_8 fractional concentrations ${}_M\boldsymbol{C_2F_6}$ and ${}_M\boldsymbol{C_3F_8}$, $\boldsymbol{X}$ kg of liquid C_2F_6 is added to $\boldsymbol{Y}$ kg of liquid C_3F_8 already in the condenser to arrive at a total liquid mass of $\boldsymbol{Z}$ kg of blended fluorocarbon liquid, such that:

$$X = \frac{{}_MC_2F_6 * 0.138 * Y}{{}_MC_3F_8 * 0.188} \tag{A.4}$$

The total number of moles, $\boldsymbol{M}$, in the liquid mixture is given by:

$$M = \frac{Z}{{}_MC_2F_6 * 0.138 + {}_MC_3F_8 * 0.188} \tag{A.5}$$

As an example, for a desired molar ratio of 95%C_3F_8/5%C_2F_6, 386 g of liquid C_2F_6 would need to be added to 10 kg liquid C_3F_8 already in the condenser tank, for a total of 56 moles.

The multi-step procedure used to create this blend is outlined below:

- *Step 1:* the mass of 10 kg, equivalent to 53.2 moles of C_3F_8 liquid transferred to the condenser of the blend machine is verified by subtraction of the tare weight of the C_3F_8 cylinder and its flexible tubing from their combined gross weight).

- *Step 2:* the overall weight of the C_2F_6 cylinder and its flexible tubing are noted;

2015 JINST 10 P03027

- *Step 3:* the condenser temperature is reduced to around -30°C, reducing the saturated vapour pressure of the C_3F_8 fluid to $\sim$ 1.36 bar_{abs}. This temperature is chosen to be significantly below the saturated vapour pressure of C_2F_6 in its uncooled cylinder ($\sim$ 27 bar_{abs} at 15°C) to allow the saturated vapour pressure in the condenser to be measured over a wide range of C_2F_6 concentrations;

- *Step 4:* 386 g of C_2F_6 is progressively transferred into the condenser reservoir, noting the change in saturated vapour pressure of the fluid mixture in the condenser — according to a prepared curve of vapour pressure *vs.* C_2F_6 concentration in C_3F_8, as illustrated on the left axis of figure 18 — together with the mass changes in the condenser and C_2F_6 cylinder. The condenser pressure is measured with a transducer having a resolution of $\pm$ 15 mbar. Small additive steps, followed by pauses of a few minutes to allow the pressure to stabilise, are made to reduce the risk of overshoot. In practice we have found that the change in saturated vapour pressure — around 68 mbar.%$[C_2F_6]^{-1}$ — to be a more precise indicator than the change in mass in the cylinder and condenser which are measured by electronic balances with a precision of $\pm$ 100 g. Nonetheless all mixtures are considered "nominal" at this stage: absolute molar mixture ratio is measured in a custom ultrasonic gas mixture analyser (step 6);

- *Step 5:* when C_2F_6 transfer is complete and confirmed by the condenser pressure at -30°C (figure 18), the condenser temperature is increased to raise the pressure to around 9 bar_{abs}, a value chosen to be within the safe range of output pressure of the compressor. The temperature necessary to achieve this for different C_2F_6/C_3F_8 molar mixtures is shown in figure 12 (right axis). The condenser pressure of 9 bar_{abs} is insufficient to supply the thermal test structures; the liquid booster pump increases the liquid pressure to around 16 bar_{abs};

- *Step 6:* the compressor is started and the blended fluid circulated through a dummy load around a short closed loop on the blending machine (figures 6, 7). In this loop the superheated vapour mixture passes through a custom ultrasonic gas mixture analyser (section 4). The molar mixture of the circulating fluid is determined to a precision of $\pm$ 0.3% from the sound velocity, which is a unique function of the molar concentrations of the two components at the measured temperature and pressure;

- *Step 7:* if the mixture corresponds to the desired ratio, circulation is started through the thermal test stand.

The mixing procedure detailed in the six preceding steps is extended when more C_2F_6 or C_3F_8 is added to an existing C_2F_6/C_3F_8 blend.

- *Step 8:* the fluorocarbon blend is recovered into the condenser tank from the external piping using the compressor. Fluorocarbon vapour (at the minimum compressor aspiration pressure of 800 $mbar_{abs}$) remaining in the external tubing is evacuated to avoid changing the mixture of the new blend once it is dispatched through the thermal test stand;

- *Step 9:* the mass, **Z'**(kg), of the fluorocarbon fluid in the condenser is noted by subtraction of the tare weight from the gross weight. Combining fluid lost in the evacuation procedure with any lost in the preceding thermal studies, (**Z - Z'**) kg of blended fluid is determined to have been lost.

2015 JINST 10 P03027

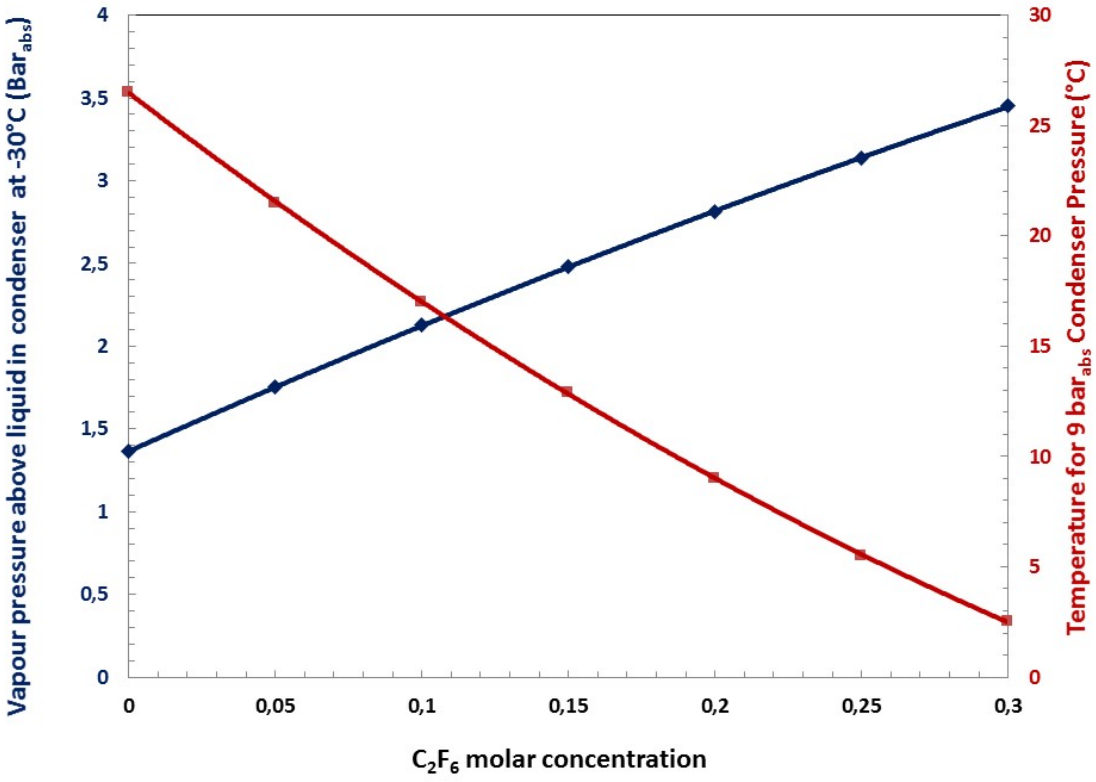

Figure 18. Saturated vapour pressure above liquid at -30°C in the condenser (left axis) and condenser temperature for a vapour pressure of 9 bar_{abs} (right axis), for a range of C_2F_6/C_3F_8 mixtures: calculated using NIST-REFRROP [8].

Note: measurements with the ultrasonic gas analyser (section 4) have shown that the mixture molar ratio is maintained despite losses during circulation. The mixing protocol makes use of the observation that losses affect the two components in proportion to their molar concentrations in the blend.

The total number of moles remaining, ***M'***, after losses and recovery is given by:

$$M' = \frac{Z'}{{}_M C_2F_6 * 0.138 + {}_M C_3F_8 * 0.188} \tag{A.6}$$

while the numbers of remaining moles of C_2F_6, $\boldsymbol{M'}_{C2F6}$ and of C_3F_8, $\boldsymbol{M'}_{C3F8}$, are given by:

$$M'_{C2F6} = M' *_M C_2F_6; \quad M'_{C2F6} = M' *_M C_3F_8 \tag{A.7}$$

- *Step 10:* the condenser temperature is reduced to -30°C. This allows the molar composition of the remaining mixture to be verified by measurement of saturated vapour pressure, and also prepares for the measurement of the molar composition of the new blend;
- *Step 11:* the numbers of moles of C_2F_6 & C_3F_8, $\boldsymbol{M'C_2F_6}$ & $\boldsymbol{M'C_3F_8}$, in the condenser form the basis for a change to a new desired blend, with C_2F_6 & C_3F_8 fractional molar

concentrations defined as ${}_M\boldsymbol{C_2F_6}$**':**${}_M\boldsymbol{C_3F_8}$**'**, created for example with the addition of a mass $\boldsymbol{A}$ kg of C_2F_6 liquid to the total liquid mass $\boldsymbol{Z'}$ (kg) in the condenser, where:

$$A = \left(\frac{{}_MC_2F_6' * M'_{C3F8}}{\left(1 - {}_MC_2F_6'\right)} - M'_{C2F6} \right) * 0.138 \tag{A.8}$$

As an example, for a new desired molar ratio of 15%C_2F_6/85%C_3F_8, 805 g of liquid C_2F_6 would need to be added to a tank containing a remaining total of 9.36 kg of blended C_3F_8 and C_2F_6 with previously-set molar ratio of 5%C_2F_6/95%C_3F_8 corresponding to *steps 1–4*. This situation might correspond to the case where 10% of the previously blended liquid had been lost due to leaks and the evacuation loss in the long tubing connecting the blend machine to the thermal test stand.

Fluid is progressively transferred into the condenser, noting mass changes in the C_2F_6 cylinder and the condenser. Small additive steps with stabilisation pauses reduce the risk of overshoot. The change in saturated vapour pressure of the fluid mixture in the condenser is verified after each step, according to a prepared curve illustrated on the left axis of figure 13. As in step 4, all mixtures are considered "nominal" at this stage: absolute molar mixture ratio is measured by the ultrasonic gas mixture analyser (step 13);

- *Step 12:* the condenser temperature is increased to raise the condenser pressure to ~ 9 bar_{abs};
- *Step 13:* the compressor is started and the blended fluid circulated through the dummy load and the ultrasonic gas mixture analyser of the blend machine The molar mixture is determined to $\pm$ 0.3% from the sound velocity;
- *Step 14:* if the mixture corresponds to the desired ratio, circulation is started through the thermal test stand.

B The ultrasonic gas mixture analysis instrument

We have developed a custom on-line instrument for the simultaneous measurement of binary gas mixture molar composition measurement and flowmetry [9]. The instrument uses the phenomenon whereby the sound velocity in a binary gas mixture at known temperature and pressure is a unique function of the molar concentration of the two components of differing molecular weight. Ultrasonic gas analysis was first used in particle physics for the analysis of the N_2/C_5F_{12} (*dodecafluoropentane*: mw = 288) Cherenkov gas radiator of the SLD Cherenkov Ring Imaging Detector [11], as a simpler alternative to on-line refractive index monitoring. Since then it has been adopted in all the major ring imaging Cherenkov detectors.

The instrument is illustrated in figure 19. A pair of capacitative ultrasonic transducers are mounted face-to-face around 666 mm apart in a flanged stainless steel tube. The sounding volume includes a 'pinched' region of inner diameter 44.3 mm. Vapour is diverted around the ultrasonic transducers by flow-deflecting cones. The temperature in the analysis tube is monitored to a precision of better than $\pm$ 0.2°C through the use of six internal NTC sensors. Pressure is monitored with a transducer having $\pm$1 mbar precision.

2015 JINST 10 P03027

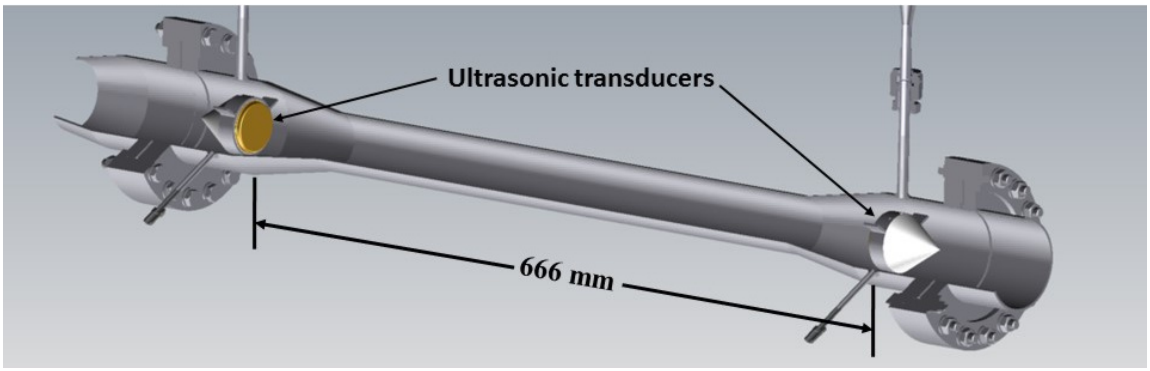

Figure 19. Internal construction of the custom ultrasonic gas mixture analyser showing the mounting of the ultrasonic transducers on their axial flow-deflecting cones. Six internal NTC thermistors are also installed (not shown). The perpendicular tubes allow pressure transducer attachment and the injection of calibration gas.

Two custom ultrasonic gas mixture analyser/flowmeters were constructed to measure the molar concentration of C_2F_6 and C_3F_8 in the blend. Identical instruments are installed at the blend recirculation machine and at a point in the return tube near the thermal test stand

Sound velocity is calculated from the transit time of sound pulses over the known path length. The molar concentration of the two component vapours is determined from a comparison of online sound velocity measurements with velocity-composition look-up table data gathered from prior measurements in calibration mixtures or from theoretical data derived according to an appropriate equation of state. The NIST-REFPROP [8] package is based on the most accurate pure fluid and mixture models currently available for a wide range of fluid combinations. It currently implements three models for the thermodynamic properties of pure fluids: equations of state explicit in Helmholtz energy, the modified Benedict-Webb-Rubin (BWR) equation of state, and an extended corresponding states (ECS) model. Mixture calculations employ a model that applies mixing rules to the Helmholtz energy of the mixture components.

Figure 20 illustrates the sound velocity measured in the instrument in varying C_2F_6/C_3F_8 molar mixing ratios at a temperature of 19.2°C and a pressure of 1.14 bar_{abs}. These calibration mixtures span the region of thermodynamic interest in this work and were set up by partial pressure ratio in the previously-evacuated tube, to create molar mixtures. Component partial pressures were set using a MKS "Baratron®" capacitative absolute pressure gauge with a precision of $\pm$ 1 mbar. The transducer foil inter-distance had been previously established using the gas calibration procedure described in [9], to a precision of $\pm$ 0.1 mm.

Individual contributions (shown in parentheses below) to the overall 0.05 ms^{-1} sound velocity measurement error (equivalent to 0.042 % of the measured sound velocity of 118.3 ms^{-1} at 20 % C_2F_6 concentration, for example) were due to:

- $\pm$ 0.2 °C temperature stability in the sonar tube (equivalent to $\pm$ 0.044 ms^{-1});
- $\pm$ 4 mbar pressure stability in the tube ($\pm$ 0.012 ms^{-1}) with blend circulation machine operating;

2015 JINST 10 P03027

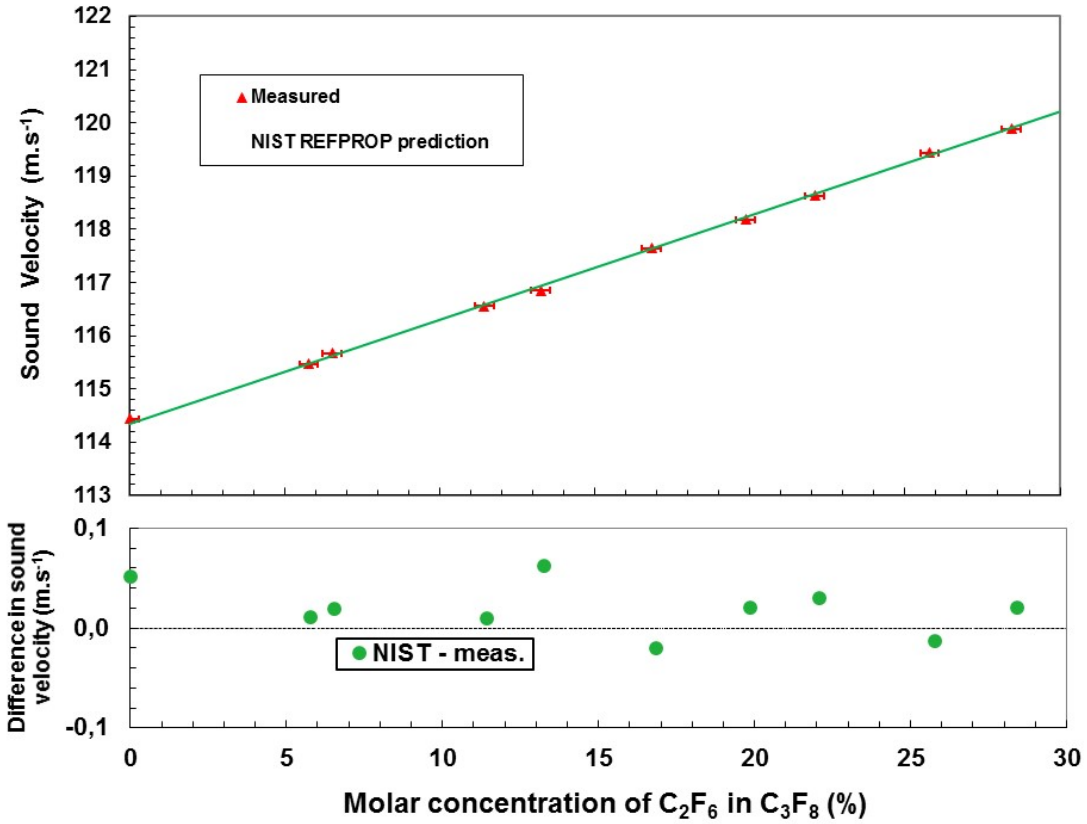

Figure 20. *Upper plot:* comparison between measured sound velocity data and theoretical predictions in NIST-REFPROP [8] for molar C_2F_6/C_3F_8 mixtures of thermodynamic interest, at 1.14 bar_{abs} & 19.2°C. The binary gas mixture measurement uncertainty of 0.3% is illustrated in red. *Lower plot:* differences between the measurements and the NIST-REFPROP predictions.

- $\pm$ 0.1 mm transducer inter-foil measurement uncertainty ($\pm$ 0.018 ms^{-1});
- $\pm$ 100 ns electronic transit time measurement uncertainty ($\pm$ 0.002 ms^{-1}).

The average difference between measured sound velocity and the NIST-REFPROP [8] predicted sound velocities in mixtures with (0 to 30 %) C_2F_6 in C_3F_8 was around 0.03 % at pressures near 1 bar_{abs} and temperatures around 19°C.

The precision of mixture determination, ∂ ***(mix)***, at any concentration of the two components is given by;

$$\partial\,(mix) = \frac{\partial c}{m} \tag{B.1}$$

where $\boldsymbol{m}$ is the local slope of the sound velocity/concentration curve and $\partial \boldsymbol{c}$ is the uncertainty in the sound velocity measurement. For example, in a blend of 20 % C_2F_6 in C_3F_8 the sound velocity uncertainty of 0.05 ms^{-1} yields a concentration uncertainty of $\sim$0.3 % at 20 %C_2F_6, where the slope is $\sim$0.18 $ms^{-1}\%.[C_2F_6]^{-1}$.

2015 JINST 10 P03027

References

[1] D. Attree et al., *The evaporative cooling system for the ATLAS inner detector*, 2008 *JINST* **3** P07003 [INSPIRE].

[2] G. Beck and G. Viehhauser, *Analytic model of thermal runaway in silicon detectors*, *Nucl. Instrum. Meth.* **A 618** (2010) 131 [INSPIRE].

[3] ATLAS collaboration, *ATLAS inner detector: technical design report,* 1, CERN-LHCC-97-016, CERN, Geneva Switzerland (1997).

[4] ATLAS collaboration, *ATLAS inner detector : technical design report,* 2, CERN-LHCC-97-017, CERN, Geneva Switzerland (1997).

[5] ATLAS collaboration, *ATLAS pixel detector: technical design report*, CERN-LHCC-98-13, CERN, Geneva Switzerland (1998) [INSPIRE].

[6] A. Bitadze, *Thermodynamical measurements for the ATLAS inner detector (evaporative cooling system)*, Ph.D. thesis, http://theses.gla.ac.uk/id/eprint/5186, Department of Physics and Astronomy, University of Glasgow, Glasgow U.K. (2013).

[7] A. Abdesselam et al., *The integration and engineering of the ATLAS semiconductor tracker barrel*, 2008 *JINST* **3** P10006 [INSPIRE].

[8] E. Lemmon, M. Huber and M. McLinden, *'REFPROP' standard reference database* 23*, version* 9.0, U.S. National Institute of Standards and Technology, U.S.A. (2010).

[9] R. Bates et al., *A combined ultrasonic flow meter and binary vapour mixture analyzer for the ATLAS silicon tracker*, 2013 *JINST* **8** P02006 [arXiv:1210.4835] [INSPIRE].

[10] *CERN UNICOS (Unified Industrial Control System) project webpage*, http://ab-project-unicos.web.cern.ch/ab-project-unicos/.

[11] G.D. Hallewell, G.D. Crawford, D.G. McShurley, G.J. Oxoby and R. Reif, *A sonar based technique for the ratiometric determination of binary gas mixtures*, *Nucl. Instrum. Meth.* **A 264** (1988) 219 [INSPIRE].

2015 JINST 10 P03027